Degradation Mechanisms of Thermal Barrier Coatings Used in Land-Based Gas Turbine Blades Exposed to Low-Grade Fuel Impurities

BY

Adeel Khalid

A Thesis Presented to the

DEANSHIP OF GRADUATE STUDIES

KING FAHD UNIVERSITY OF PETROLEUM & MINERALS

DHAHRAN, SAUDI ARABIA

In Partial Fulfillment of the
Requirements for the Degree of

MASTER OF SCIENCE

In

MECHANICAL ENGINEERING

June, 2011

KING FAHD UNIVERSITY OF PETROLEUM & MINERALS

DHAHRAN 31261, SAUDI ARABIA

DEANSHIP OF GRADUATE STUDIES

This thesis, written by Adeel Khalid under the direction of his thesis advisor and approved by his thesis committee, has been presented to and accepted by the Dean of Graduate Studies, in partial fulfillment of the requirements for the degree of **MASTER OF SCIENCE IN MECHANICAL ENGINEERING.**

Thesis Committee

Dr. Zuhair M. Gasem (Advisor)

Dr. Abul Fazal M. Arif (Member)

Dr. Nasser Al Aqeeli (Member)

for

Dr. Amro M. Al- Qutub
Department Chairman

Dr. Salam A. Zummo
Dean of Graduate Studies

2/7/11

Date

Dedicated

To

My Family

ACKNOWLEDGMENTS

In the name of ALLAH, the Most Beneficent, the Most Merciful.

Praise and gratitude to ALLAH, the Almighty, with whose gracious help, I was able to complete this work with patience and endurance.

Acknowledgement is due to King Fahd University of Petroleum and Minerals, Saudi Arabia for providing the support and also for the Center for Clean Water and Clear Energy at MIT and KFUPM.

I am deeply grateful to my thesis advisor Dr. Zuhair M. Gasem for his support, guidance and encouragement throughout this study. His wide knowledge and logical way of thinking have been great value for me. I would also like to thank my committee members Dr. Abul Fazal M. Arif and Dr. Nasser Al Aqeeli for their reviews and comments.

I would also like to thank the staff Materials Science lab specially Mr. Latif Hashmi and Mr. Saleh Al Abbas for their help during the experimental work.

Very special thanks to parents and other family members for their unconditional and endless support, love, sacrifices, prayers and understanding throughout my academic career. You all have been a constant support for me and showed never wavering belief in me and understanding during the last 2 years.

I am grateful to all my colleagues for their help and friendship especially to Mr. Abdullah Gujba, Mr. Danish Ahmed and Mr. Aqeel Mirza. I want to express my thanks to some of my dearest friends specially Salman, Yousaf, Monim, Ahmed, Babar, Sarmad, Saad, Nauman, Faraz and all others for their friendship and for giving me much needed bout of laughter.

Table of Contents

List of Tables

List of Figures

THESIS ABSTRACT

Name **Adeel Khalid**

Thesis Title **Degradation Mechanisms of Thermal Barrier Coatings Used in Land-Based Gas Turbine Blades Exposed To Low Grade Fuel Impurities.**

Degree **Masters of Science**

Major Field **Mechanical Engineering**

Date of Degree **June 2011**

Thermal barrier coating (TBC) systems are widely used in gas turbines to provide thermal insulation and oxidation resistance for hot-gas path components. There is a growing trend in the local power generation industry to use low-grade fuels and lightly treated crude oil to drive industrial turbine engines in order to meet the increasing power demand at reasonable cost. Land-based turbines burning low grade fuels are susceptible to different modes of hot corrosion depending on the operating temperature and the dominant fuel impurities. Low grade Saudi fuels usually contain high concentrations of sulfur, sodium, and vanadium which can form salts of Na_2SO_4, V_2O_5, and NaCl after combustion. The molten salts deposit on the first stage turbine blades and vanes and induce different types of degradation on various layers of TBCs including the ceramic-based top coat, the metallic-based bond coat, and the interface between the top and bond coats. The effects of Na_2SO_4, NaCl, and V_2O_5 corrosive salts on the microstructure and life of air-plasma sprayed (APS) TBC's have been investigated in the present research. The examined TBC's consisted of ZrO_2 top-coat stabilized by 8% Y_2O_3, Ni-25%Cr-10%Al-0.6%Y bond-coat, and IN718 substrate. Various salt compositions have been examined: 75 wt.% Na_2SO_4 + 25 wt.% V_2O_5, 75 wt.% Na_2SO_4 + 25 wt.% NaCl, 75 wt.% Na_2SO_4, and 25 wt.% NaCl. Each specimen was sprayed with the salt of interest and exposed isothermally at 900 °C for different time periods over a span of 1200 hours. The microstructure and life of TBC specimens exposed to pure oxidation environment were used as bench marks.

خـــلاصـــــة الرســـــــالـــــــة

اسم الطالب : **عـديل خالـد**

عنوان الرسالة: **جـــراداتيون ميشانيســـمس أف ثيرمـــال بـــرير ســـتنجز أســـد إن لاندباســـيد جـــس .تـــوربين لاديـــس كسبوســـيد طـــه لـــو جـــراد فـــول مبـــوريتييس**
التخصص: هندسه **ميكانيكيـــــة**

تاريخ الرساله: جون ٢٠١١

وتستخدم على نطاق واسع الحرارية طلاء الجدار (TBC) نظم في توربينات الغاز لتوفير العزل الحراري ومقاو مة الأكسدةلمكونات مسار الغاز الساخن. هناك اتجاه متزايد في صناعة توليد الطاقة المحلية على استخدام الوقود على منخفض الدرجة والنفط الخام يعامل باستخفاف لدفع المحركات التوربينية الصناعية من أجل تلبية زيادة الطلب على الطاقة بتكلفة معقولة. البريةتوربينات احتراق الوقود بدرجة منخفضة عرضة لأنماط مختلفة من التآكل الساخن ا عتمادا على درجة حرارة التشغيلوالشوائب الوقود المهيمن. انخفاض الوقود السعودية الصف عادة ما تحتوي عل ى تركيزات عالية من الصوديوم والكبريت والفاناديوم التي يمكن أن تشكل أملاح Na_2SO_4، V_2O_5،وكلوريدا صوديوم بعد الاحتراق. إيداع الأملاح المنصهرةعلى ريش التوربينات المرحلة الأولى ودوارات وحمل أنواع مختلف ة من التدهور على طبقات مختلفة من معطف TBCs بما في ذلك السيراميك مقرها العلوي،ومعطف السنت المسند دة المعدنية، والتفاعل بين أعلى والمعاطف السندات. آثارNa_2SO_4، كلوريد الصوديوم، وتآكل أملاح V_2O_5 على المجهرية وحياة الهواء رش البلازما (APS) وقد تم التحقيقفي TBC في البحث الحالي. تألفت لفحTBC ZrO_2لأ على معطف استقر بنسبة Y_2O_3، ني - 25 - 10 ٪الكروم ٪ Y آل 0.6 ٪ السندات معطف، والركيزة IN718. وقد تم فحص التراكيب المختلفة الملح : 75 ٪ بالوزنNa_2SO_4 + 25 ٪ بالوزن V_2O_5، و 75 ٪ وزن Na_2SO_4ر كلو بالوزن كلوريد_الصوديوم، وNa_2SO_4، ووزن 25 ٪ كلوريد الصوديوم. تم رش كل عينة مع الملح منلاهتمام و تتعرض ل يرمـالسـوث لفترات زمنية مختلفة علىمدى 1200 ساعة. استخدمت المجهرية والحياة العينTBC يتع رض للبيئة نقية كماالأكسدة علامات مقاعد البدلاء.

CHAPTER 1 INTRODUCTION

Thermal barrier coatings (TBCs) are widely used in hot-gas path components of gas turbines to reduce thermal effect and increase turbine service life. The use of TBCs can result in temperature reduction of 200^{o}C at the metal surface, thereby improving the integrity of the metal component and enhancing engine performance. The TBC system is usually composed of a MCrAlY bond coat (M=Ni, Co) as an oxidation resistant layer and yttria-stabilized zirconia (YSZ) as a topcoat that provides thermal insulation for the metallic substrate. There are different failure modes that lead to spallation of TBCs such as excessive oxidation and hot corrosion which reduce the durability of the coatings. Low quality fuels usually contain impurities such as sulfur and vanadium which can form Na_2SO_4 and V_2O_5 molten salts on the surface of turbine blades. Such fused salts can react with the TBC and are detrimental for the stability of TBC system. During high temperature exposure of TBCs, an oxide layer is formed at the top coat and bond coat interface which is described as thermally grown oxide (TGO). As the oxides grow (which depends on many factors [1–3]), they cause compressive residual stresses leading to TBC failure near the ceramic topcoat/TGO/bond coat interfaces. In addition, a mismatch between coefficient of thermal expansion of bond coat and ceramic topcoat can increase coating failure during thermal cycles. The general expectation of higher gas turbine efficiency in future definitely requires in-depth understanding of all factors influencing TBC failure and lifetime.

It is recognized that a basic understanding of TBC materials and failure must be gained if TBCs are to achieve their full potential of being designed and applied to last the life-time of the component. This has been the focus of intense research activity in the past decade

[4]. The complexity and diversity of TBC structures and severity of operating conditions make this a challenging task. TBC is perhaps the only system where a complex interplay occurs of all the following phenomena: diffusion, oxidation, phase transformation, elastic deformation, plastic deformation, creep deformation, thermal expansion, thermal conduction, fracture, fatigue and sintering. In this framework, microstructure characterization and description of the failure modes is a pre-requisite for life time modeling.

Motivation & objectives

A large number of power plants in the Kingdom of Saudi Arabia use low grad/crude oil for power generation. The low grade/crude oil contains impurities which react to form fused salts. At higher temperatures these corrosive impurity salts lead to increased high temperature corrosion damage (hot corrosion) which can cause catastrophic failures of TBC system.

The aim of this research is to investigate the effect of fuel impurity salts on the integrity and performance of top coat, bond coat, and top coat/bond coat interfaces in a typical TBC used in the local power generation industry.

CHAPTER 2 LITERATURE REVIEW

2.1 Modern Gas Turbines

Thermal barrier coating systems (TBCs) are widely used in modern gas turbine engines to lower the metal surface temperature in the combustor and turbine section hardware. Engines for both aero-jet propulsion and land-based industrial power generation have taken advantage of this technology to meet increasing demands for greater fuel efficiency, lower NOx emissions, and higher power and thrust. The engine components exposed to the most extreme temperatures are the combustor and the initial rotor blades and nozzle guide vanes of the high-pressure turbine. Metal temperature reductions of up to 200^{o}C are possible when TBCs are used in conjunction with external film cooling and internal component air cooling [5]. A diagram of the relative temperature reduction achieved using both TBC and cooling air technologies on hot section hardware is shown in Figure 2.1.1

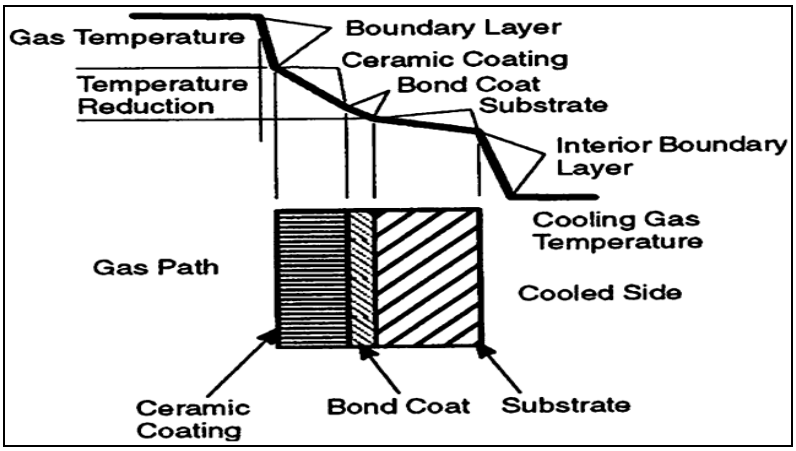

Figure 2.1.1 Schematic of a TBC on an air-cooled gas turbine engine component [5].

2.2 Thermal Barrier Coating System

Typical thermal barrier coatings (TBCs) consist of a ceramic overlay coating (ZrO_2, stabilized by 7-8% Y_2O_3) and an aluminum-rich oxidation resistant metallic layer, also called bond coat, deposited onto the Ni-based substrate. The bond coat is normally a MCrAlY (where "M" is Ni or Co). The ceramic top coat is deposited either by atmospheric plasma spraying (APS) [6] or by electron-beam physical vapor deposition (EB-PVD) [7]. Figure 2.2.1 shows the schematic of typical microstructure formed in case of APS and EB-PVD sprayed TBC. The Al_2O_3 TGO provides oxidation resistance to the underneath bond coat elements.

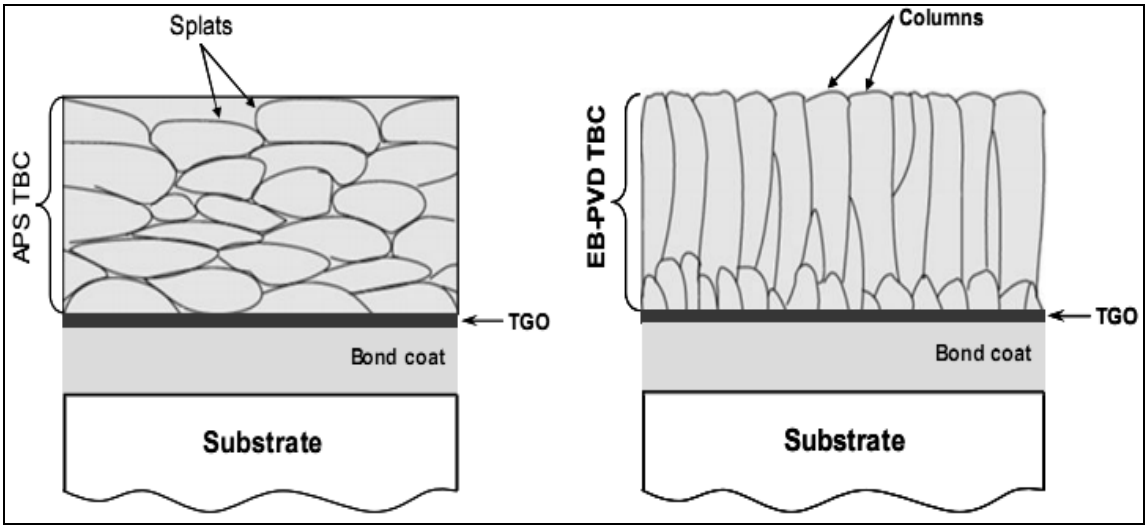

Figure 2.2.1 Schematic of TBC microstructure in a thermal barrier coatings deposited by APS and EB-PVD techniques [6, 7].

2.2.1 Ceramic top coat

In order to withstand high thermal and mechanical loading during service thermal barrier ceramic coatings must possess low thermal conductivity, high temperature resistance, appropriate thermal expansion coefficient, strain tolerance, chemical stability, corrosion and oxidation resistance. ZrO_2 has a low thermal conductivity at elevated temperature as shown in Figure 2.2.2 in combination with a high thermal-expansion coefficient $9–11.5 \cdot 10^{-6}$ K^{-1}, which is not too far from the value of underlying substrate ($\sim 12 \cdot 10^{-6}$ K^{-1}). ZrO_2 is the base material of choice for the ceramic top-coats of high temperature components [8].

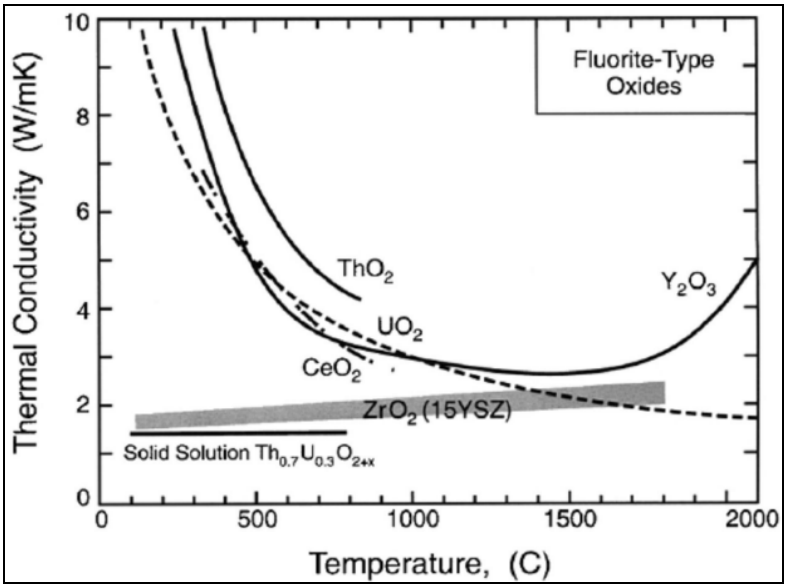

Figure 2.2.2 The thermal conductivity of several ceramic materials, including ZrO_2 [9]

Depending on temperature, pure ZrO_2 can exist in different crystallographic modifications, as shown in the phase diagram of ZrO_2-Y_2O_3 in Figure 2.2.3. Between the melting point 2680°C and 2370°C pure zirconia has a cubic symmetry. Tetragonal

structure is stable in the temperature interval between 2370°C and 1170°C. During cooling down at temperatures below 1170°C martensitic transformation to monoclinic phase takes place with a volume expansion of about 4 vol.% [10]. To prevent this, oxides (dopants), such as Y_2O_3, CaO, Sc_2O_3, Yb_2O_3 and MgO are normally added to zirconia to stabilize the high temperature cubic or tetragonal phases. 7 wt% Y_2O_3 partially stabilized ZrO_2 (7YSZ) is by far the most applied material for top coat [8, 10].

The two methods of YSZ deposition (EB-PVD and APS) produce not only different microstructures as shown in Figure 2.2.4, but also result in various properties of the coating [11].

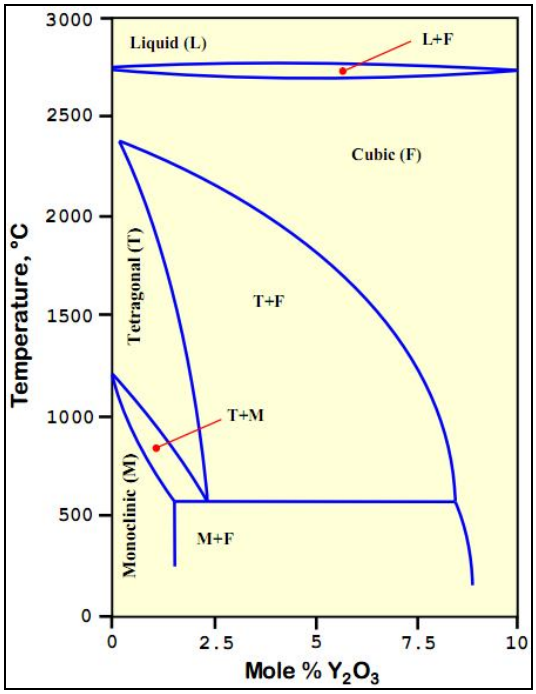

Figure 2.2.3 Phase diagram ZrO_2-Y_2O_3 [12]

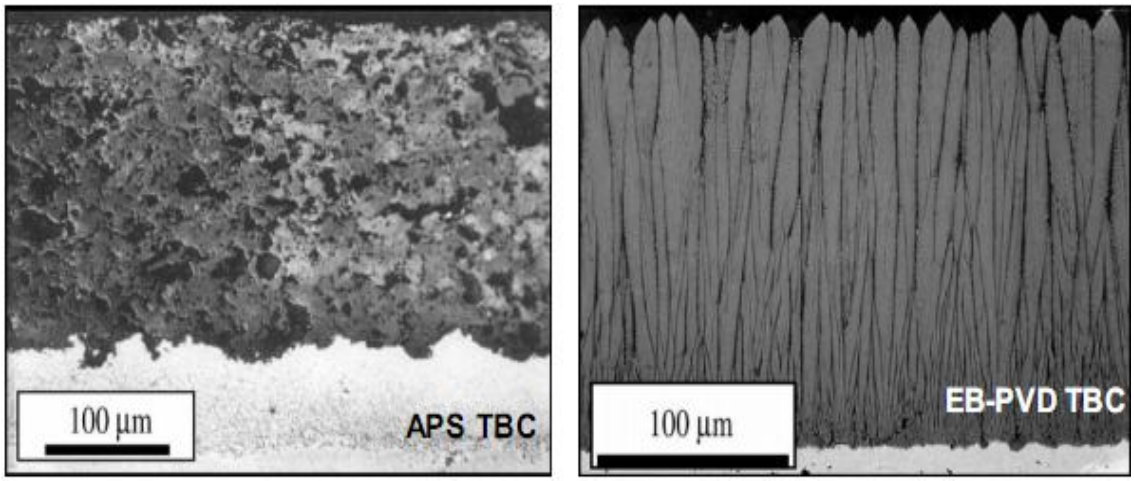

Figure 2.2.4 Cross-sections of plasma-sprayed and EB-PVD ZrO_2-8wt%Y_2O_3 [11]

2.2.1.1 Air Plasma Sprayed top coat

During the process solid particles are injected into a plasma jet. There they are heated up to temperatures of more than 4000°C, melt and are accelerated towards

the substrate by an electrostatic field. There are three main modes of plasma spraying: air plasma (APS), vacuum plasma (VPS) and low pressure plasma spraying (LPPS). Ceramic coatings, such as YSZ are usually deposited in air. The following parameters may influence the final microstructure of deposited coating: density of the ceramic powder, particle sizes, particle morphologies, melting point (the powder can be melted not completely), temperature, velocity of the particles, etc. A low substrate temperature between 100 and 300°C is typically chosen [13, 14].

The thickness of a plasma sprayed coatings may reach several millimeters, however, APS TBCs mostly have a thicknesses below 0.5 mm. Normally, the plasma sprayed coatings exhibit a lamellar morphology of the spraying splats (thickness – 1 to 10 μm, diameter – 200 to 400 μm) [16]. The inter splat boundaries, gaps and cracks are essentially oriented parallel to the bond coat interface as shown in Figure 2.2.5 porosity up to 25 vol. % can thus be obtained [15].

The microstructure of plasma sprayed coatings contains many defects, e.g. large globular pores as well as micro-cracks between and within the individual splats. The orientation of the cracks and pores normal to the heat flow reduces the thermal conductivity of the ceramic coating from 2.3 $W*m^{-1}*K^{-1}$ for a fully dense YSZ-material to 0.8 – 1.7 $W*m^{-1}*K^{-1}$ [16].

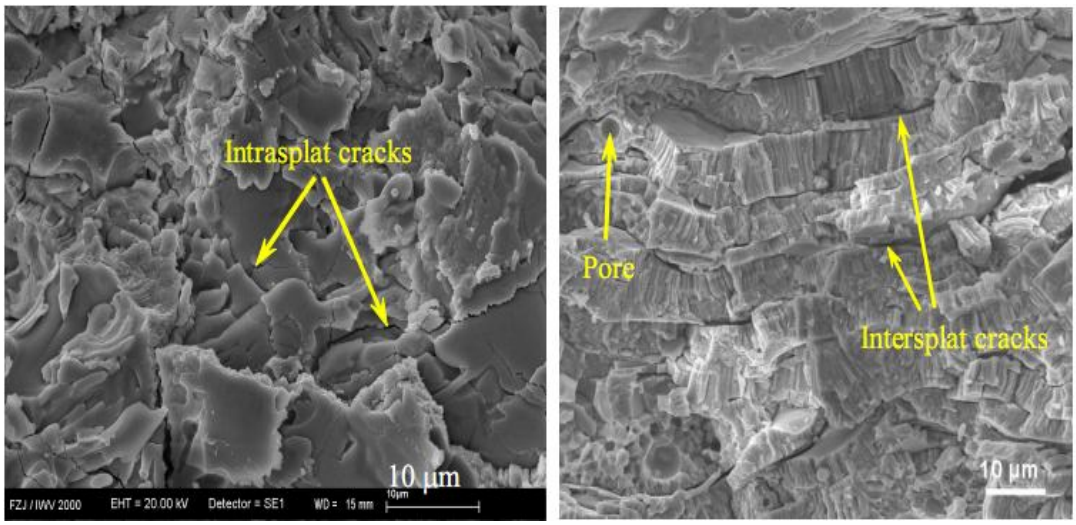

Figure 2.2.5 Cross-sections of plasma-sprayed and APS ZrO_2-8wt%Y_2O_3 [16].

2.2.1.2 Electron Beam-Physical Vapor Deposition (EB-PVD) top coat

In contrast, TBCs deposited by EB-PVD have a columnar microstructure as shown in Fig.2.2.1. The columnar grains are oriented predominantly parallel to the vapor flux and normal to the substrate surface [17]. In the EB-PVD process, focused high-energy electron beams generated from electron guns are directed to melt and evaporate ingots as well as to preheat the substrate inside the vacuum chamber. The vapor cloud condenses on the rotating component and forms the coating. The solidified particles have a limited mobility because of the low thermal energy of the vapor species, leading to shadowing effect and formation of layers within the columns, resulting in a typical feather-like structure [18]. The disconnected columns impart excellent strain tolerance, accommodating thermal expansion mismatch. The bond coat surface is kept smooth for deposition, since PVD process provides good chemical bonding [19].

2.2.2 Metallic Bond Coat

The bond coat provides protection of the base material against oxidation attack and hot gas corrosion. The bond coat also provides the adhesion between substrate and TBC. Three main groups of bond coats are currently state-of-the-art: diffusion aluminide, platinum aluminide and overlay MCrAlY bond coats. All types of metallic coatings feature a high content of Al, which enables the formation of a stable Al_2O_3 scale providing good oxidation resistance. The alumina-TGO has a low growth rate, a dense hexagonal close-packed crystal structure, which is stable between room temperature and melting point. In addition to oxidation/corrosion protection, the bond coat, which is ductile at high temperature, also provides significant compensation of the thermal expansion misfit between the metallic substrate and the ceramic top coat [20]. The bond coat is applied by either APS or vacuum plasma spraying.

2.2.2.1 Diffusion Aluminide

Diffusion aluminide coatings are based on the intermetallic compound β-NiAl. Pack cementation is a commonly used process, because it is relatively inexpensive and capable of coating many small parts in one batch. The parts are immersed in a powder mixture, containing alumina and aluminum particles, and ammonium halide activator. Coating takes place at temperatures between 800 and 1000^{o}C. Aluminum halides react on the surface of the part and deposit aluminum. More advanced processes consist of ‘‘over the pack’’ vapor phase aluminizing (VPA) or chemical vapor deposition (CVD). These processes can control the flow of the aluminum halides to selected areas of the parts to be coated, and are used especially when there is a need to coat also the internals of components.

Depending on the activity of the aluminum and the coating temperature, one can achieve two coating microstructures [21]. The low activity, high-temperature process (1050-1100^{o}C), forms NiAl by outward diffusion of nickel. In the high activity, low temperature process (700-950^{o}C), Ni_2Al_3 and possibly β-NiAl forms by inward diffusion of aluminum. Typically a diffusion heat treatment is applied to form a fully homogeneous β-NiAl layer [22].

2.2.2.2 Platinum Aluminide

The addition of platinum to the diffusion aluminide coating system is beneficial in two ways: first, the platinum enhances the diffusion of aluminum [23] into the substrate alloy during the diffusion aluminizing process. Platinum aluminide can also be made either with the low activity, high-temperature process or by the high activity—low-temperature diffusion process. Figures 2.2.6 and 2.2.7 show schematically the microstructures of these two types of coatings. Since the part surface is grit blasted prior to the application of the platinum, grit inclusions can serve as markers to indicate the additive coating layer or the original alloy surface. In the case of the low activity—high-temperature process, the additive layer is above the nickel diffusion zone, and in the case of high activity—low-temperature process, the additive layer is under the original surface marked by the grit inclusions. The relative thickness of the nickel diffusion zone also indicates the degree of outward diffusion of nickel. As the coating grows inwardly in the high activity, low-temperature process, it traps the carbides and other inclusions near the original alloys surface, as shown in Figure 2.2.7. These inclusions can have a deleterious effect in that they can lower the oxidation/corrosion resistance of the coating. In either processes,

platinum aluminide can be single phase ((Ni, Pt)-Al) or double phase ((Ni, Pt)-Al + $PtAl_2$) [22].

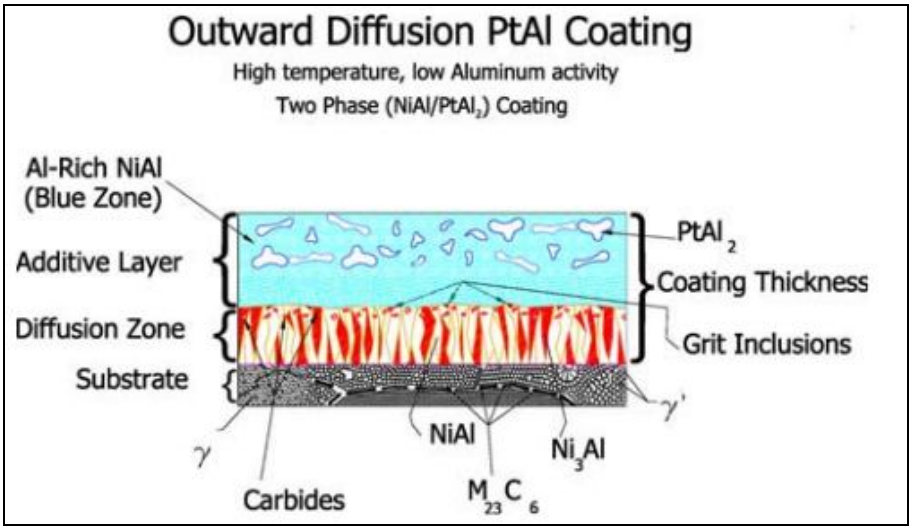

Figure 1.2.6 Microstructure schematic showing platinum aluminide formed from a low activity, high-temperature process [22].

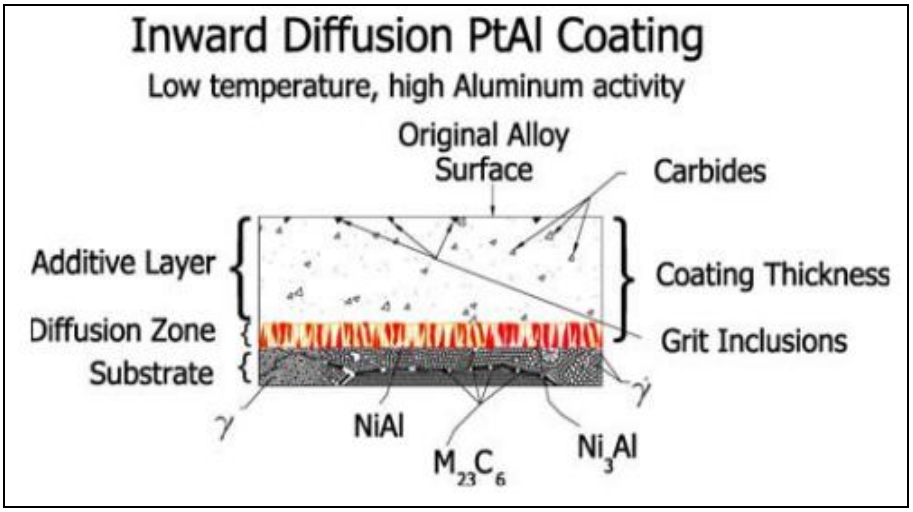

Figure 2.2.7 Microstructure schematic showing platinum aluminide formed from a high activity, low-temperature process [22].

2.2.2.3 MCrAly Bond coat

The microstructure and chemical properties of MCrAlY coatings are less sensitive to the chemical composition of the base material. The "M" of MCrAlY stands for either Ni or Co, or a combination of both, depending on the type of superalloy. Figure 2.2.8 compares corrosion and oxidation resistance of different bond coats with increasing chromium content.

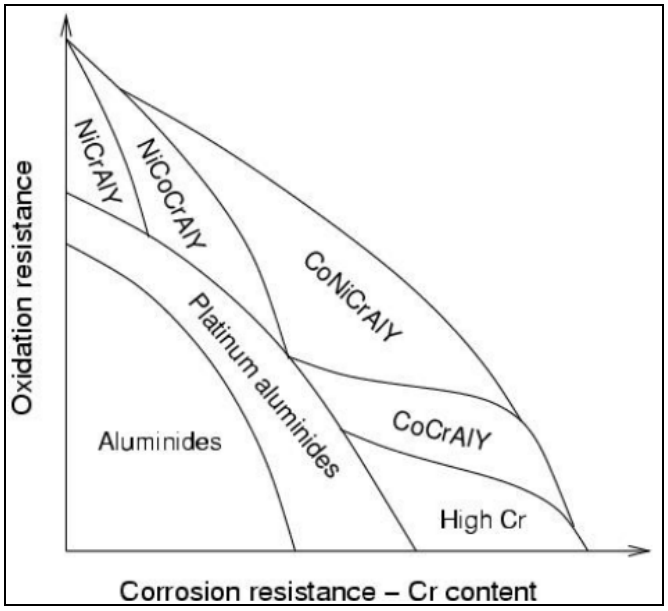

Figure 2.2.8 Comparative corrosion and oxidation resistance of bond coats [24]

Different mechanisms have been proposed to explain the beneficial effect of Y on the growth and adherence of Al_2O_3 scales forming in the bond coat, such as: increasing scale plasticity [25], grading the differences between mechanical properties of the scale and the substrate [26], modification of the scale growth mechanism [27] and improving chemical bonding between the scale and the substrate [28]. However, there are several

studies, which demonstrate that Y can be detrimental for oxide adherence [29, 30]. Yttrium incorporates in the compact alumina TGO scale and as a result of internal oxidation forms Y_2O_3 precipitations, which is accompanied by Y-depletion process in MCrAlY bond coat. If the yttrium concentration has been decreased beneath a critical level, its positive effect on TGO adherence is lost, resulting in TGO spallation [31]. Addition of another reactive element, like Hf plays a similar role.

2.3 Limiting factors in TBC Performance

2.3.1 Bond coat oxidation (TGO Growth)

Under service conditions turbine components with TBCs are exposed to an oxidation of the bond coat. Continuous transport of oxygen through the ceramic top coat is the source as shown in Figure 2.3.1. The resulting formation of a compact Al_2O_3 scale along the bond coat / top coat interface provides a high oxidation resistance and protects the metal from further oxidation. On the other hand lateral growth of the TGO results in addition with thermal stresses in a large in-plane compressive stress (up to 3 GPa at room temperature). Significant out-of-plane tensile stresses are induced and delamination cracks parallel to the interface are generated as soon as even small curvatures of the interface are present. Failure usually occurs upon cooling because the thermal mismatch between top coat, TGO and bond coat generates additional in-plane compressive stresses. For this reason, the morphology, adherence and stresses in the TGO are important issues in TBC evaluation and life prediction [32-34].

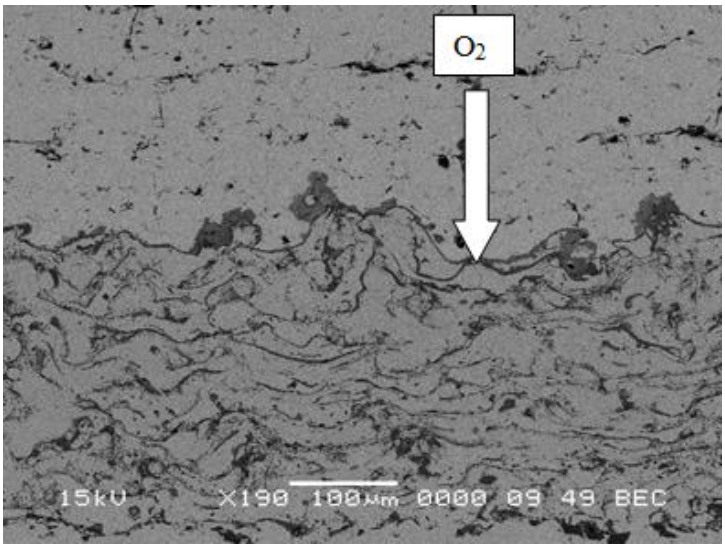

Figure 2.3.1 Diffusion of O_2 through the ceramic top coat towards the interface

In a TBC system the oxidation behavior of the bond coat is determined by its chemical composition [35]. For MCrAlY type bond coat TGO scale consists mostly of Al_2O_3. Stable, slow growing Al_2O_3 normally originates around 900°C for NiCrAlY bond coats. The growth rate of the oxide scale is controlled by the inward transport of oxygen along grain boundaries towards the interface between TGO and bond coat (i.e., internal oxidation) [36], as well as by the outward diffusion of Al cations along the grain boundaries of alumina in order to react with oxygen anions at the interface between TGO and ceramic top coat, i.e., external oxidation [37, 38]. Internal oxidation can lead to the volume expansion of the complete oxide scale and significant compressive stresses of about 1-2 GPa [39], which play an important role for the adhesion of oxide scale[40].

2.3.2 Top coat degradation by hot corrosion

Hot corrosion is one of the main destructive failure modes in thermal barrier coatings (TBCs) which come as a result of molten salt effect on the coating–gas interface. Low quality fuels usually contain impurities such as Na and V which can form Na_2SO_4 and V_2O_5 salt on the surface of turbine blades. Such fused salts can react with yttria (the stabilizer component of YSZ) and cause transformation of tetragonal or cubic zirconia to monoclinic phase during cooling. This transformation is accompanied by 3–5% volume expansion, leading to cracking and spallation of TBCs.

The mechanism of degradation during hot corrosion can be explained by the following reactions [41, 42]

$$\mathbf{V_2O_5 + Na_2SO_4 \rightarrow 2(NaVO_3) + SO_3} \quad \textbf{(2.1)}$$

$$\mathbf{ZrO_2(Y_2O_3) + 2(NaVO_3) \rightarrow ZrO_2\ (monoclinic) + 2YVO_4 + Na_2O} \quad \textbf{(2.2)}$$

Usually $NaVO_3$ is formed after the reaction of initial salts (V_2O_5 + Na_2SO_4), then $NaVO_3$ reacts withY_2O_3 to produce monoclinic ZrO_2, YVO_4 and Na_2O. But Na was detected by Chen et al.'s investigation [43] on hot corrosion of plasma sprayed Al_2O_3 and ZrO_2 coatings in molten Na_2SO_4, and it was suggested the following reactions:

$$\mathbf{Na_2SO_4 \rightarrow Na_2O + SO_3} \quad \textbf{(2.3)}$$

$$\mathbf{Al_2O_3 + Na_2O \rightarrow 2NaAlO_2} \quad \textbf{(2.4)}$$

According to Eq. (2.4), $NaAlO_2$ can be formed on the surface of Al_2O_3 particles, so that the hot corrosion rate of Al_2O_3 coating in molten Na_2SO_4 was much lower than the ZrO_2 coating.

The hot corrosion behavior and failure mechanism of TBCs comprises the following [42, 44].

a. Molten salt penetration through microcracks and open porosities.

b. Reaction of molten salt with the stabilizer of zirconia (Y_2O_3)

c. Phase transformation of zirconia from tetragonal to monoclinic, due to the depletion of stabilizer, which is accompanied by volume expansion of the coating.

d. Formation of YVO_4 crystals with rod shape that grow to outward of surface and cause additional stresses in the coating as shown in Figure 2.3.2.

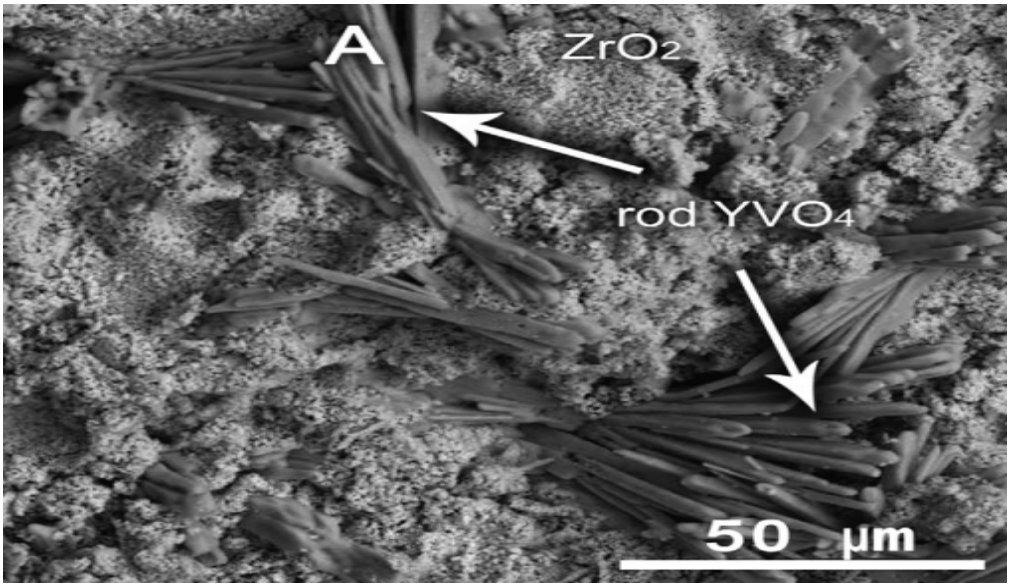

Figure 2.3.2 SEM micrograph of YVO_4 crystals on the surface of coatings [45].

2.3.2.1 Type I Hot Corrosion

This form of hot corrosion is observed [46] mainly within the temperature range 800–950°C. High temperature hot corrosion (HTHC) starts with the condensation of fused alkali metal salts on the surface of the components. A cycle of subsequent chemical reactions takes place, initially attacking the protective oxide film and progressing to deplete the chromium element from the substrate materials. With chromium depletion, oxidation of the base material accelerates and porous scale begins to form [22].

The macroscopic appearance of HTHC is characterized in many cases by severe peeling of metal and by significant color changes. For instance, a greenish tone appears on the surface of metals and alloys due to the formation of NiO in the area of accelerated attack. Microscopically, the morphology of Type I is characterized by a sulphidation and depletion region beneath the porous, non-protective scale. The reaction products frequently exhibit oxide precipitates dispersed in the salt film [22].

2.3.2.2 Type II Hot Corrosion

Low temperature hot-corrosion (LTHC) is observed [46, 47] mainly within the temperature range 650–800°C. Type II is characterized by a pitting attack in localized areas. The localized nature of attack is related to localized failure of the scale as a result of thermal cycling, erosion or chemical reactions. As opposed to Type I hot corrosion, in Type II corrosion neither microscopic sulphidation nor chromium depletion is generally observed [46]

2.3.3 Sulphidation

When the sulfur activity (partial pressure, concentration) of the gaseous environment is sufficiently high, sulfide phases, instead of oxide phases, can be formed. In the majority of environments encountered in practice by oxidation resistant-alloys, Al_2O_3 should form in preference to any sulfides, and destructive sulfidation attack occurs mainly at sites where the protective oxide has broken down. The role of sulfur, once it has entered the bond coat, appears to form Cr and Al sulfides and redistributing the protective TGO forming elements near the bond coat surface and thus interfering with the process of formation and reformation of protective TGO. If sufficient sulfur enters the bond coat so that all immediately available Al is converted to sulfides, then the less stable sulfides of base metal may form because of morphological and kinetic reasons [48].

2.3.4 Interdiffusion between substrate and bond coat

MCrAlY coatings have higher Cr and Al contents than the superalloy substrates to promote the formation of a protective oxide scales. This results in elemental diffusion of these elements from the coating to the substrate at elevated temperatures. On the other hand, the underlying superalloy has a greater content of Ni, Ti and refractory elements such as Ta, W, Mo and Re mainly to improve the high temperature mechanical properties. Consequently these elements diffuse from the substrate into the coating. The inter-diffusion between Ni-base superalloys and MCrAlY bond coatings can lead to the formation of detrimental phases, such as σ (sigma) phase, laves phases, brittle carbides [49], voids and porosity [50].

2.3.5 Sources of Salts

The sources of corrosive salts are impurities present in dirty fuel/crude oil such as Na, V and S which at high temperature react to form Na_2SO_4, V_2O_5 and NaCl. Marine environment also contains NaCl. Table 2.1 lists typical concentrations of impurities found in Saudi crude and distillate fuels.

Table 2.1 Showing typical quantities of impurities in Saudi crude and distillate samples.

Impurity	Distillate	Crude
Sulfur (%)	**0.87**	**2-3.5**
Na (ppm)	**<0.5**	**1-1.62**
K (ppm)	**<0.5**	**0.1-0.47**
V (ppm)	**0.5**	**10-15.8**
Pb (ppm)	**<1.7**	**0.1-1.7**
Ca (ppm)	**<1**	**0.1-6.6**
Ni	**<1**	**4-5.6**
Fe	**<0.5**	**0.1-1.4**

CHAPTER 3 EXPERIMENTAL PROCEDURE AND SPECIMEN PREPARATION

3.1 TBC System

The TBC sheet was provided by MIT research partners in USA. The substrate used in TBC system was Nickel based superalloy IN 718. The bond coat used was NiCrAlY and Yttria stabilized zirconia was used as a ceramic top coat. Figure 3.1.1 shows the schematic of TBC and relatives thicknesses of top coat and bond coat. Table 3.1 illustrates the composition of TBC layers and substrate.

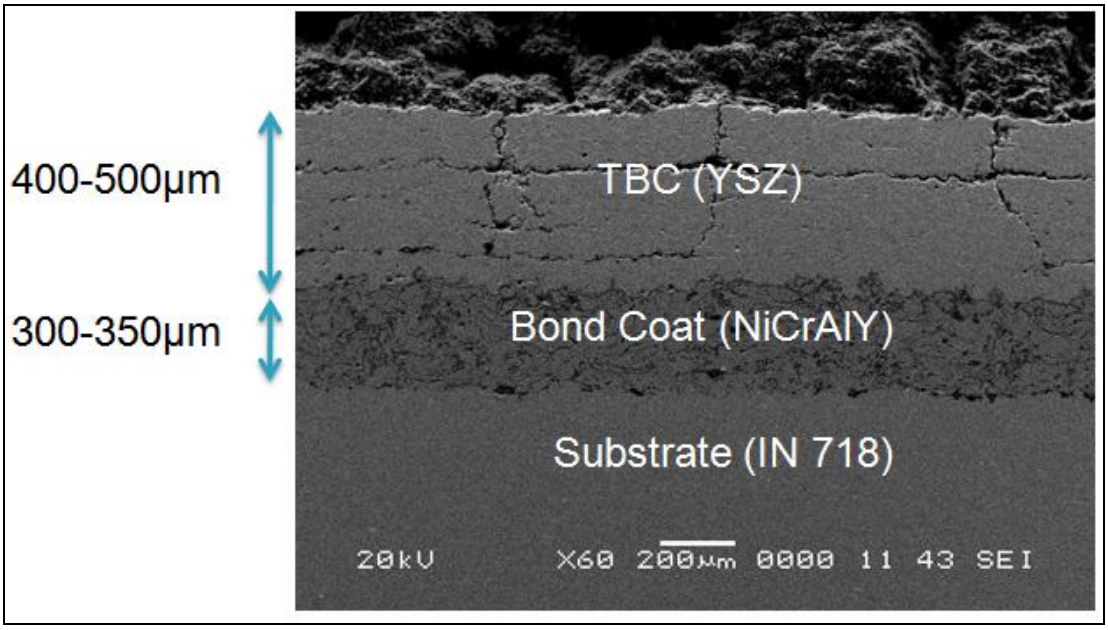

Figure 3.1.1 Schematic of TBC system showing three different layers.

Table 3.1: Compositions of TBC layers and substrate.

IN 718	Bond coat	Top coat
Balance -Ni	Balance-Ni	Balance-ZrO_2
19% Cr	25% Cr	8% Y_2O_3
18% Fe	10% Al	
0.9% Ti	0.6% Y	
5% Nb		
0.5% Al		

3.2 Specimen Preparation

The TBC coated sheet was cut into rectangular specimens of 20mm x 15mm size using water jet cutting to avoid high temperature and obtain precision cutting. The specimens were coated with salt and exposed isothermally for hot corrosion tests. Two salt mixtures were prepared in distilled water to simulate the in-service salts formation. Salt mixture A consisted of 75 wt% Na_2SO_4 and 25 wt% V_2O_5 and salt mixture B contained 75 wt% Na_2SO_4 and 25 wt% NaCl that means 75 grams of Na_2SO_4 and 25 grams of either NaCl or V_2O_5 were mixed in 100 ml of distilled water . Table 3.2 shows the composition of two salt mixtures. All the TBC specimens were cleaned in acetone and methanol before application of salt. Specimens were preheated to 200^oC before application of the salt. The surface of specimens was sprayed with salt solutions in a concentration of 20-25 mg/cm^2. The specimens were cooled and then measurements were done using micro balance. Table 3.3 presents the density and melting points of the salts used.

Table 3.2: Salt mixture compositions

Salt mixture	Wt %	Wt %
A	Na_2SO_4 (75)	V_2O_5 (25)
B	Na_2SO_4 (75)	NaCl (25)

Table 3.3: Physical specifications of salts [Oxford MSDS].

Type of salt	Density (g/cm^3)	Melting point (^oC)
Na_2SO_4	2.7	884
NaCl	2.165	801
V_2O_5	3.357	690

3.3 Exposure Procedure

For hot corrosion tests, the salt-sprayed specimens were put in an electric box furnace with air atmosphere, as shown in Figure 3.3.1, at 900^{o}C for 200, 400, 700, 1000 and 1200 hours and then cooled inside the furnace. Another set of TBC specimens, without any sprayed-salt, were placed in the furnace for same experimental conditions as the salt-sprayed samples. The isothermal exposure conditions for different TBC specimens are presented in Table 3.4.

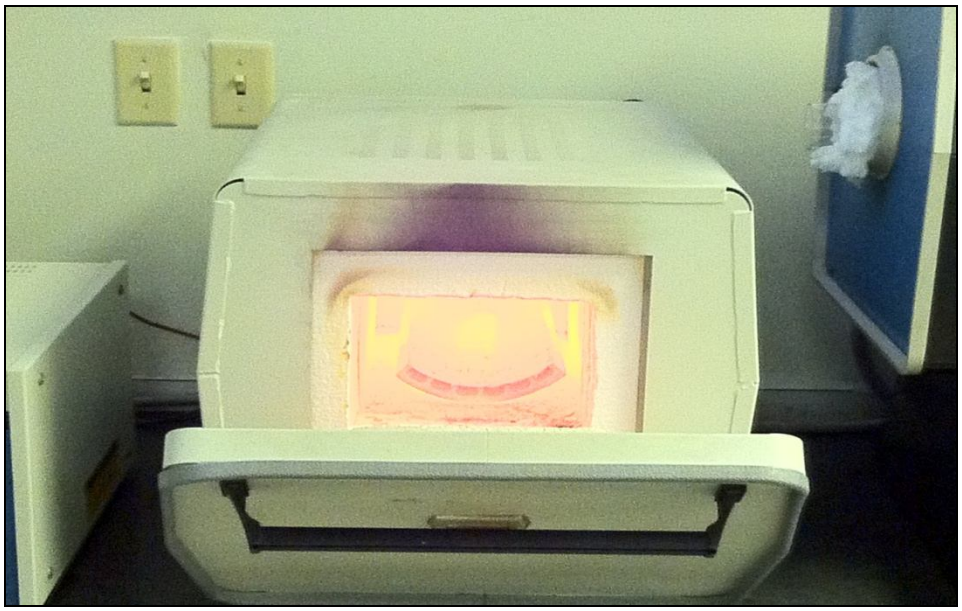

Figure 3.3.1 TBC specimens in a box furnace at 900^{o}C.

Table 3.4: Experimental conditions for isothermal exposure at 900^{o}C.

Sample #	Time (hours)	$Na_2SO_4 + V_2O_5$ Salt mixture A	$Na_2SO_4 + NaCl$ Salt mixture B	No-Salt (Pure oxidation)
1	200	○	○	
2	400	○	○	○
3	700	○	○	○
4	1000		○	○
5	1100		○	
6	1200		○	○

3.4 Microstructure Characterization

After the high temperature exposure the TBC specimens were analyzed using characterization techniques such as Scanning Electron Microscopy (SEM) in back-scattered mode, Energy-dispersive X-ray spectroscopy (EDS) and XRD. The SEM used was JEOL, Japan equipped with EDS-Oxford Instruments, UK. SEM has maximum magnification of X300,000 and is equipped with EDS element analysis. X-Ray Diffractometer was XRD-D8 Advance, manufactured by Bruker, Germany. XRD was done to study any phase change after isothermal exposure and different phases present as a result of hot corrosion.

CHAPTER 4 EXPERIMENTAL RESULTS

4.1 As-Received TBC Specimen

Figure 4.1.1 exhibits the SEM image of as-received TBC specimen and Table 4.1 lists the EDS analysis performed on this specimen. Figure 4.1.1 shows the typical TBC system consisting of a yttria stabilized zirconia (YSZ) top coat, NiCrAlY bond coat and a Nickel-based superalloy IN-718. The bond coat consists of NiCrAlY alloy and Al_2O_3 splats with compositions shown in Table 4.1.

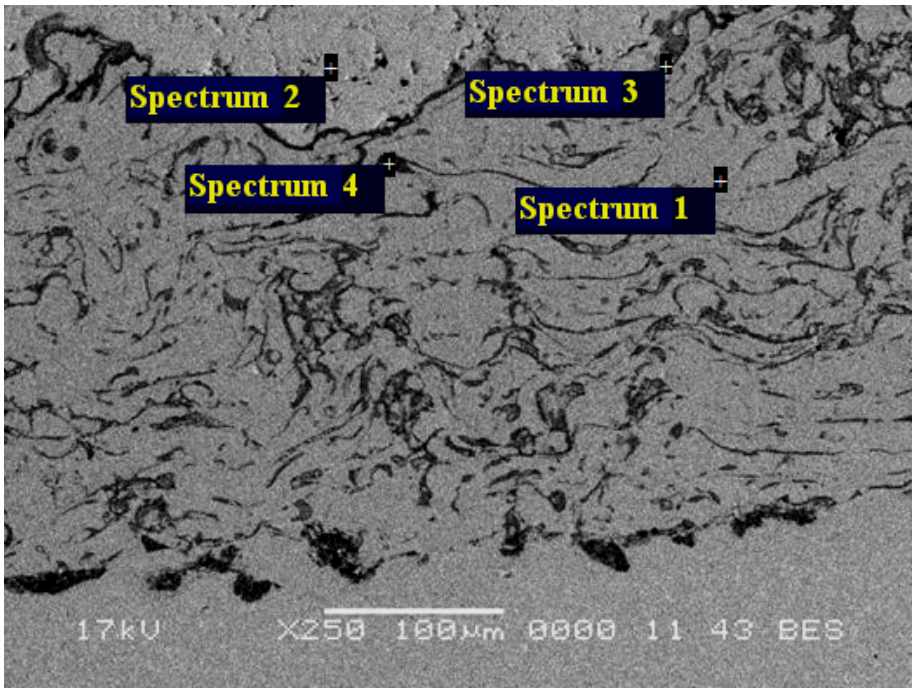

Figure 4.1.1 SEM micrograph of as-received TBC specimen.

Figure 4.1.2 shows the XRD pattern from the top surface of as-received specimen showing the peaks of tetragonal zirconia. Figure 4.1.3 demonstrates the X-ray maps of

Table 4.1: EDS analysis of as-received sample.

Point	O	Al	Cr	Ni	Zr	Y	Total
1	0	9.28	25.48	64.31	0	0.93	100
2	17.35	0	0	0	75.73	6.92	100
3	25.36	68.47	2.34	3.83	0	0	100
4	37.98	51.74	4.58	5.7	0	0	100

the as-received TBC specimen demonstrating Y and Zr in the top coat and Ni, Cr, Al,Y and O distribution in the bond coat. X-ray maps show the bond coat rich in Ni and Cr and alumina splats can also be observed in bond coat. A continuous alumina TGO layer can also be observed at the bond coat/ top coat interface.

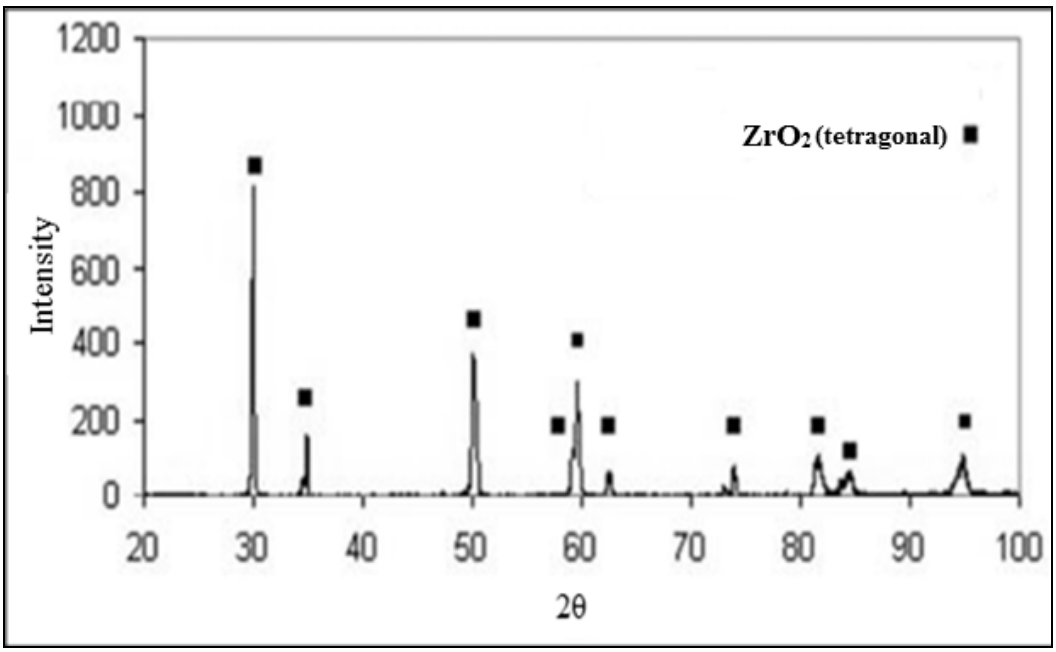

Figure 4.1.2 XRD pattern of the as-received specimen.

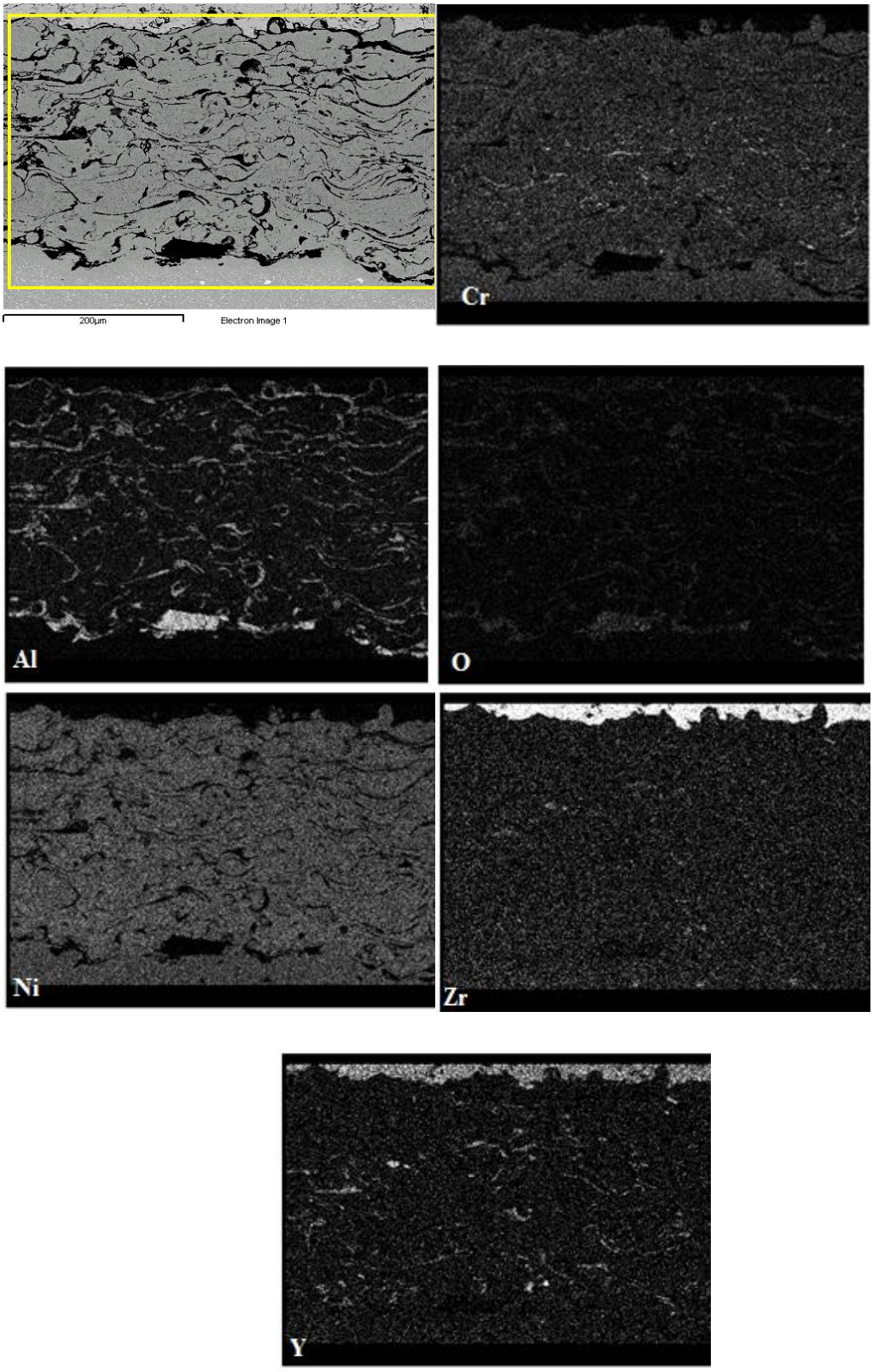

Figure 4.1.3 Elemental distribution of as-received TBC specimen.

4.2 Oxidation

Specimens without any salt mixture sprayed were exposed isothermally for 400,700, 1000 and 1200 hours at 900^{o}C. Figures 4.2.1, 4.2.2 and 4.2.3 illustrate the SEM cross-section images after isothermal exposure for 400, 700 and 1000 hours respectively. Figure 4.2.4 reveals the X-ray mapping of the specimen exposed for 1000 hours at 900^{o}C demonstrating the Al_2O_3 TGO layer at the interface. Figure 4.2.5 shows the X-ray mapping of specimen exposed isothermally for 1200 hours at 900^{o}C where thickening of the Al_2O_3 TGO can be observed at the interface with time. The TGO observed in these specimens was Al_2O_3 which was acting as diffusion barrier therefore there was no oxidation observed underneath the bond coat in these specimens. No interface cracking was observed at the top coat and bond coat interface. Also, no delamination of the bond coat was observed. Therefore it is observed that in the absence of salt mixtures, slow high temperature oxidation of bond coat and no delamination of top coat were happening.

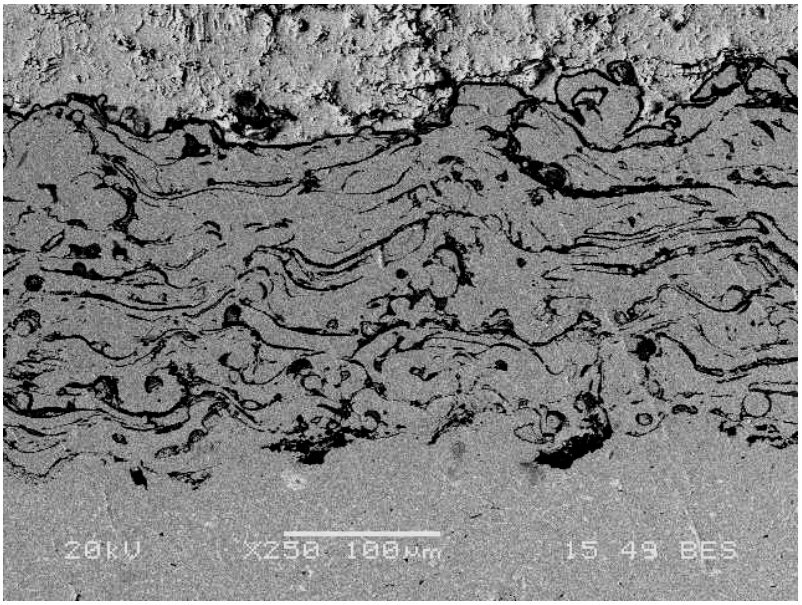

Figure 4.2.1 Back-scattered SEM Cross-section image of no-sprayed salt (pure oxidation) specimen after 400 hours at 900^{o}C.

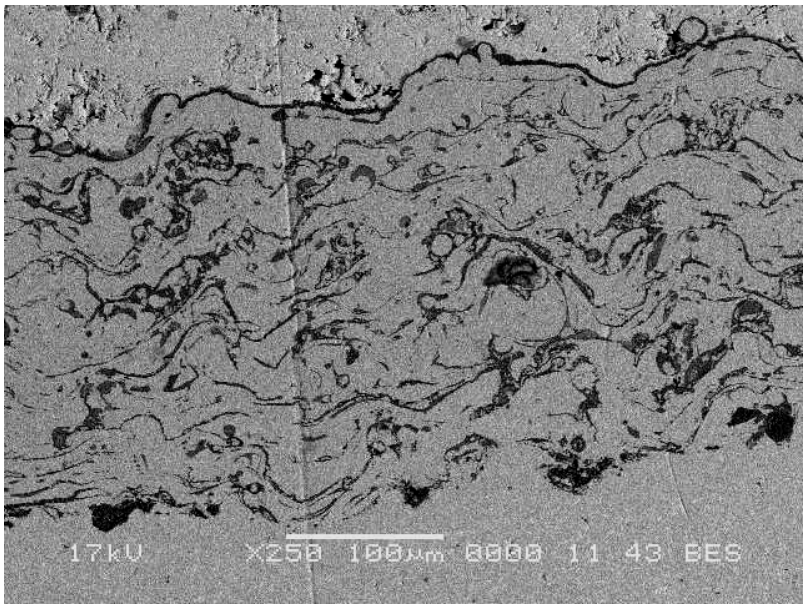

Figure 4.2.2 Back-scattered SEM cross-section image of no-sprayed salt (pure oxidation) specimen after 700 hours at 900^{o}C.

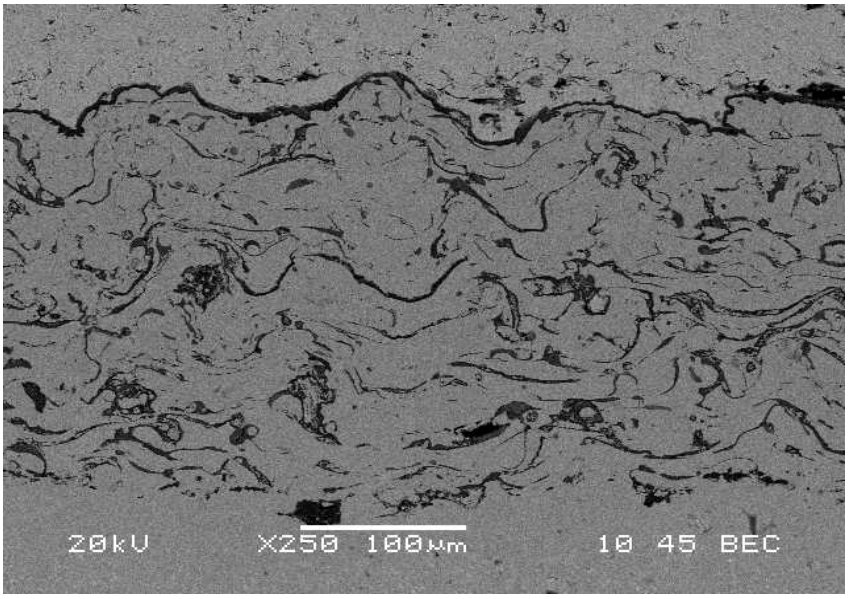

Figure 4.2.3 Back-scattered SEM cross-section image of no-sprayed salt (pure oxidation) specimen after 1000 hours at 900^{o}C.

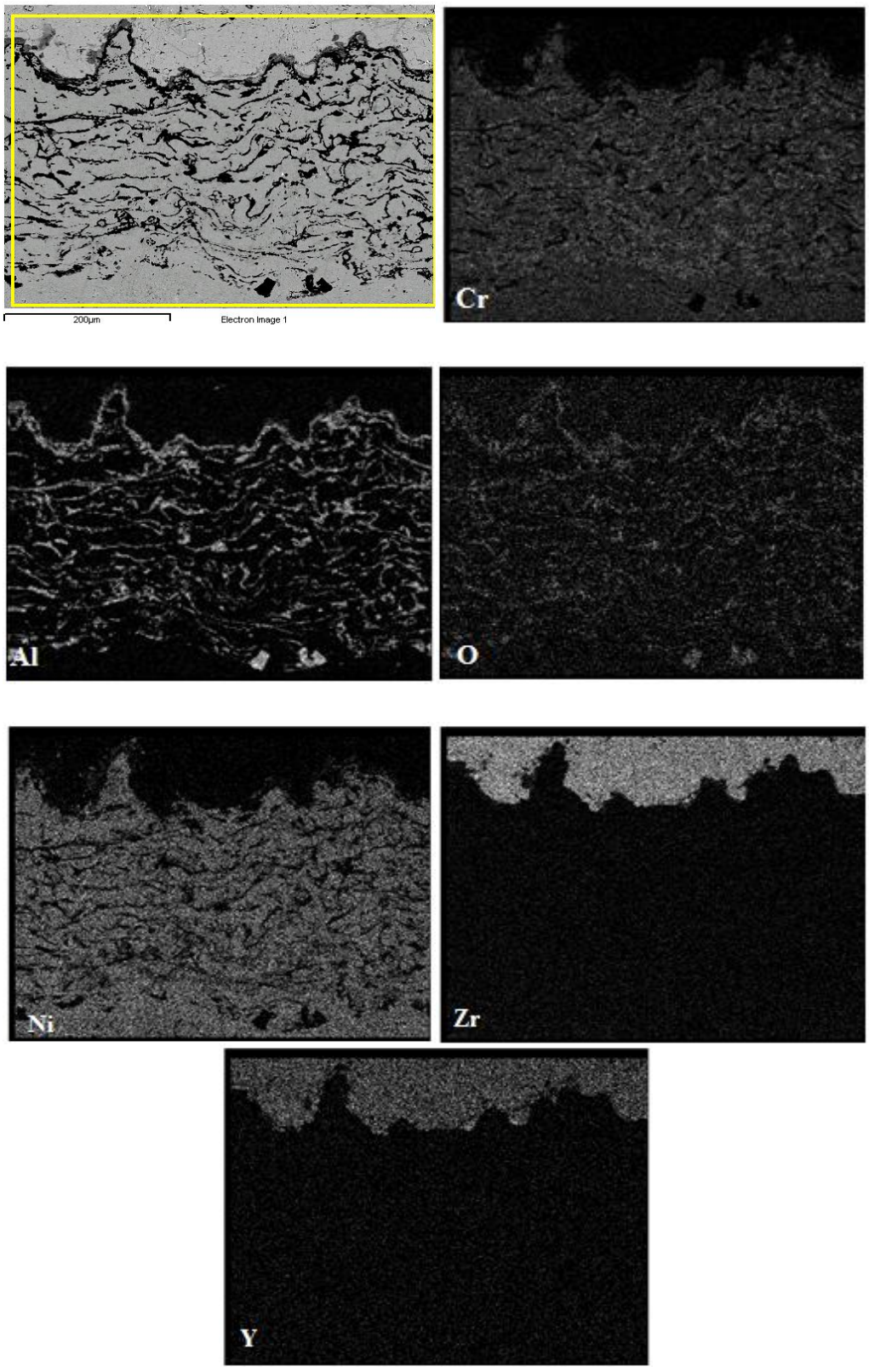

Figure 4.2.4 X-ray mapping of pure oxidation specimen at atmospheric pressure after 1000 hours at 900^{o}C.

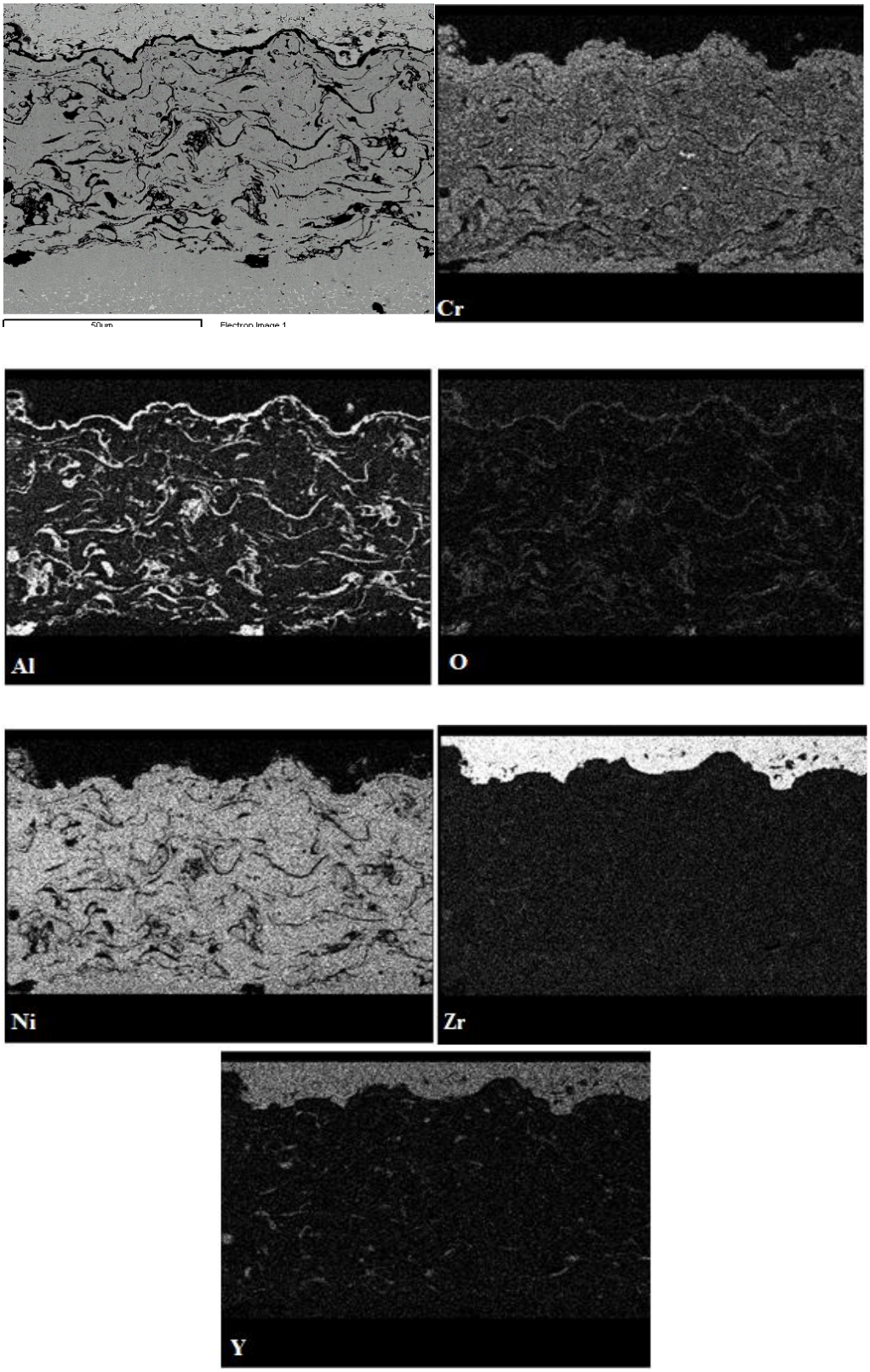

Figure 4.2.5 X-ray mapping of pure oxidation specimen at atmospheric pressure after 1200 hours at 900^{o}C.

4.3 Salt Mixture A (75% Na_2SO_4 +25% V_2O_5)

Specimens sprayed with salt mixture A were isothermally exposed for 200, 400 and 700 hours at 900°C. Al and O react to form Al_2O_3 at the bond coat/YSZ interface because they have high affinity for each other. The SEM cross-section image of specimen exposed at 200°C is presented in Figure 4.3.1. No cracking was observed at the bond coat/ top coat interface and there was no delamination of top coat.

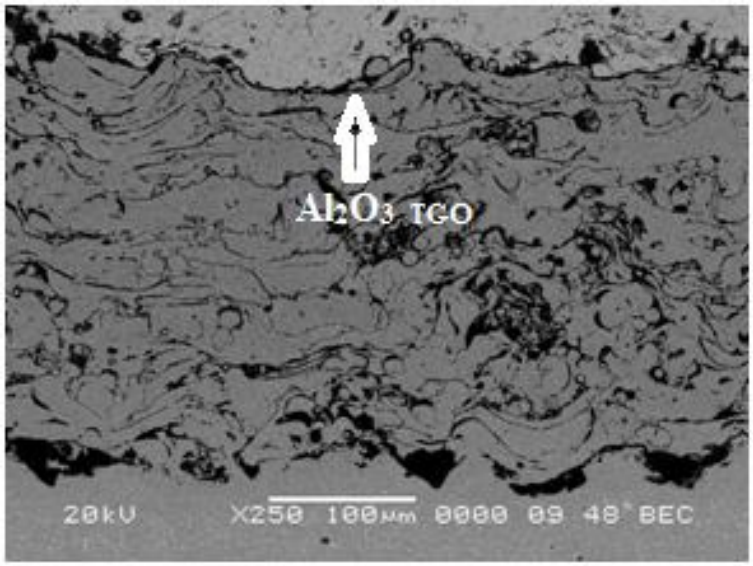

Figure 4.3.1 Back-scattered SEM cross-section image of salt mixture A specimen exposed for 200 hours at 900°C.

Table 4.2: EDS analysis of TGO shown in Figure 4.3.1.

Specimen	Point	Al	O	Cr	Ni
After 200 hrs.	TGO	65.02	26.20	4.51	4.27

However topcoat delamination and interface cracking started to appear in specimen exposed to 400 hours as observed in Figure 4.3.2 and complete spallation of top coat, sprayed with salt mixture A, was observed after 700 hours of isothermal exposure as depicted in Figure 4.3.3.

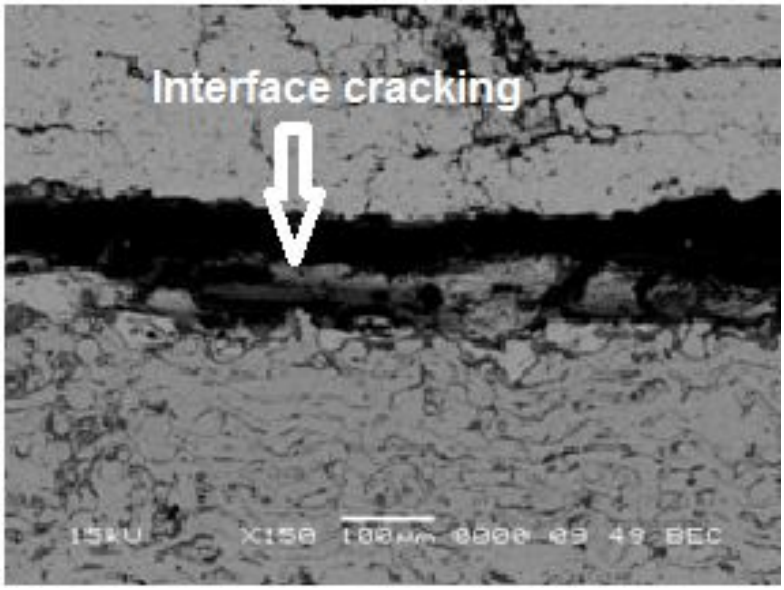

Figure 4.3.2 Back-scattered SEM cross-section image showing interface cracking after 400 hours at 900^{o}C using salt mixture A

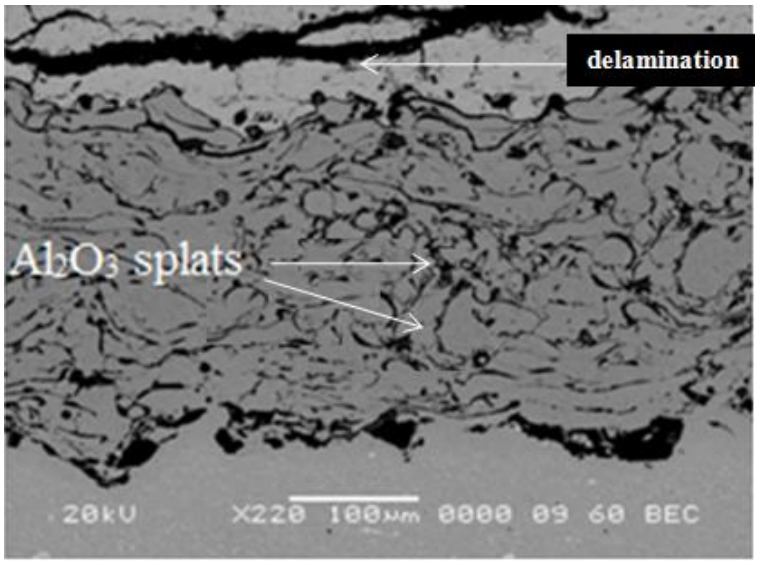

Figure 4.3.3 Back-scattered SEM cross-section image of salt mixture A showing delamination in the top coat after 700 hours at 900^{o}C.

Figure 4.3.4 exhibits the XRD pattern of specimen exposed for 400 hours and sprayed with salt mixture. XRD reveals the peaks for tetragonal and monoclinic zirconia. Rod like YVO_4 particles were observed on the surface as revealed in Figures 4.3.5 and 4.3.6

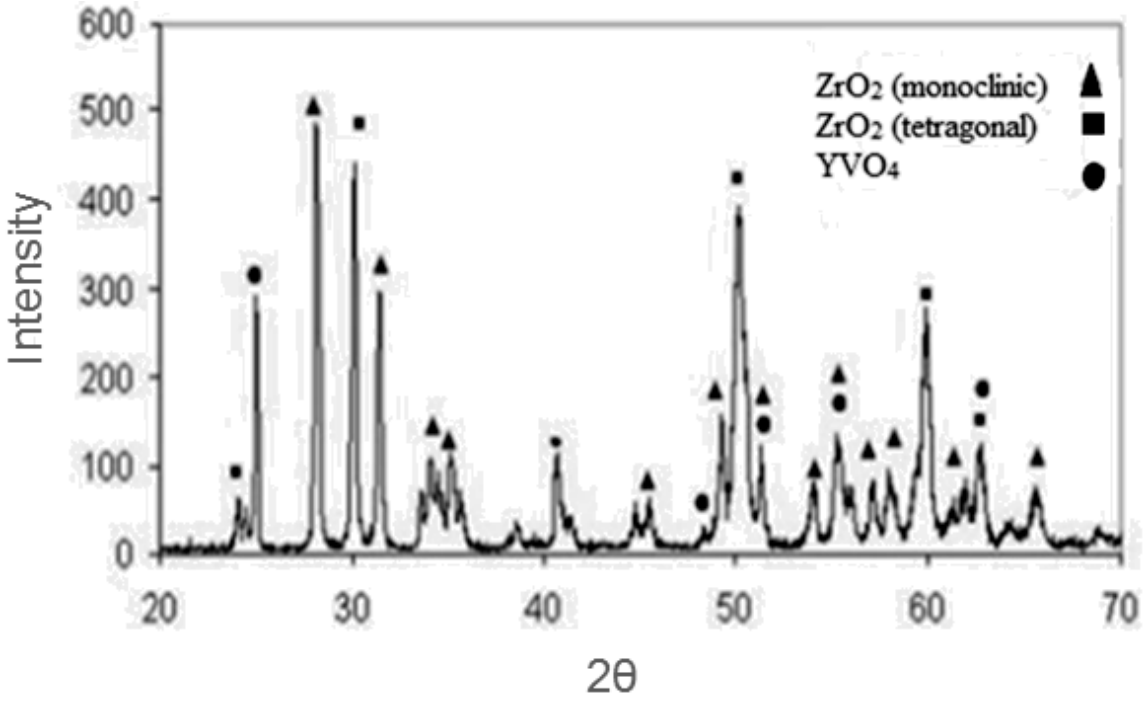

Figure 4.3.4 XRD pattern for the top surface of salt mixture A specimen after 400 hours.

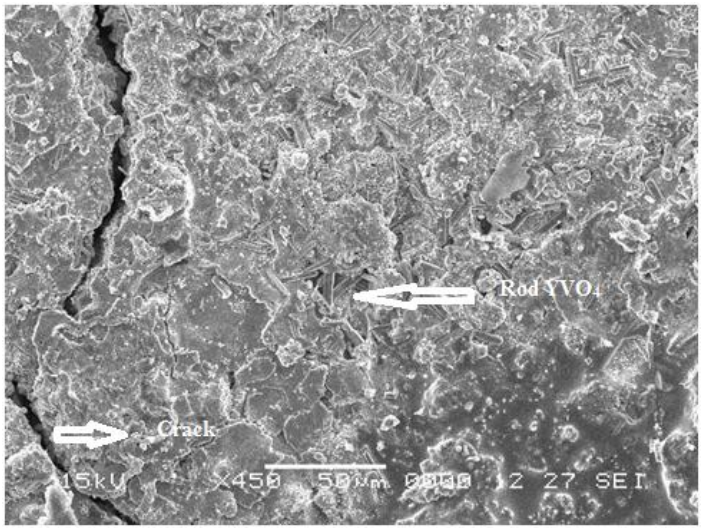

Figure 4.3.5 SEM image of the top surface of salt mixture A specimen showing crack and rod like YVO_4 after 400^oC at 900^oC.

Figure 4.3.6 SEM image of top surface of salt mixture A specimen at higher magnification showing rod like YVO_4 particles at surface after 400^oC at 900^oC.

4.4 Salt mixture B (75% Na_2SO_4 + 25% NaCl)

Specimens sprayed with salt mixture B were exposed isothermally at 900^{o}C for 200,400,700, 1000, 1100 and 1200 hours.

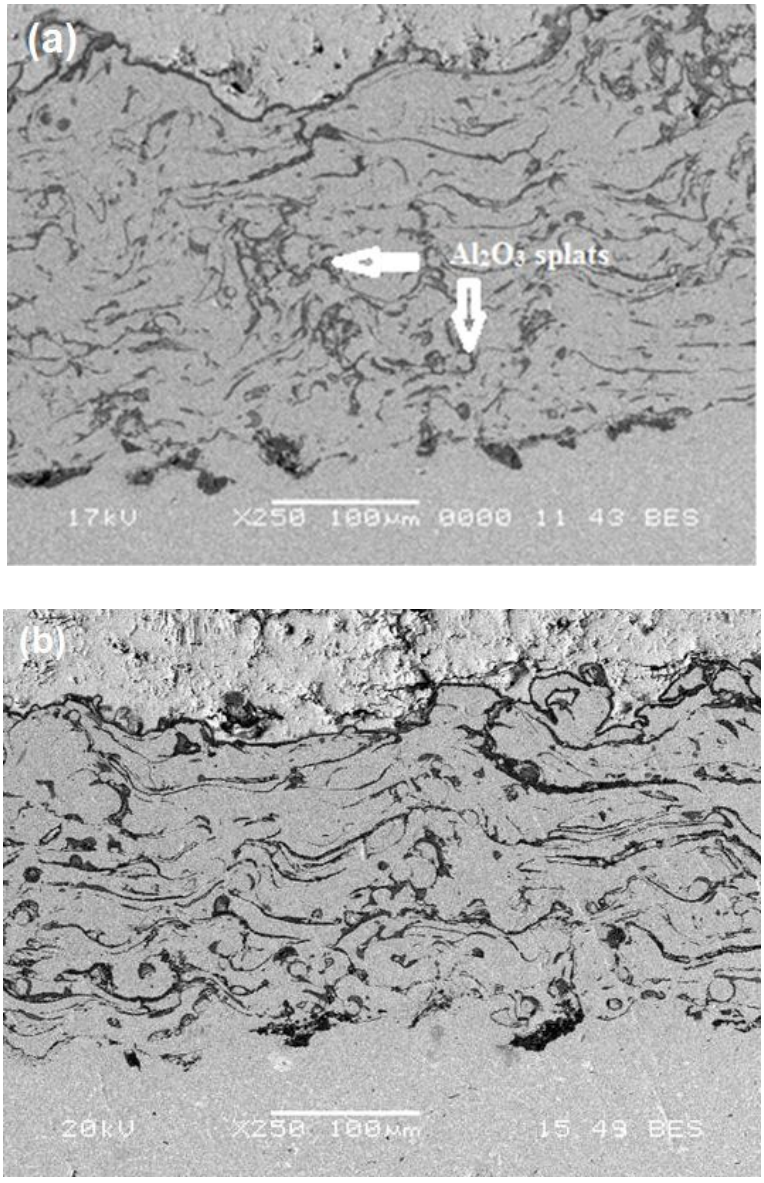

Figure 4.4.1 Back-scattered SEM cross-sectional micrographs of specimens sprayed with salt mixture B (75% Na_2SO_4 + 25% NaCl) after isothermal exposure: (a) 200 hours (b) 400 hours.

Figures 4.4.1 (a) and (b) demonstrate the SEM cross-section image of specimens that were exposed for 200 and 400 hours isothermally. Here TGO is thin layer of Al_2O_3. There was no delamination or spallation of the coating observed in these samples.

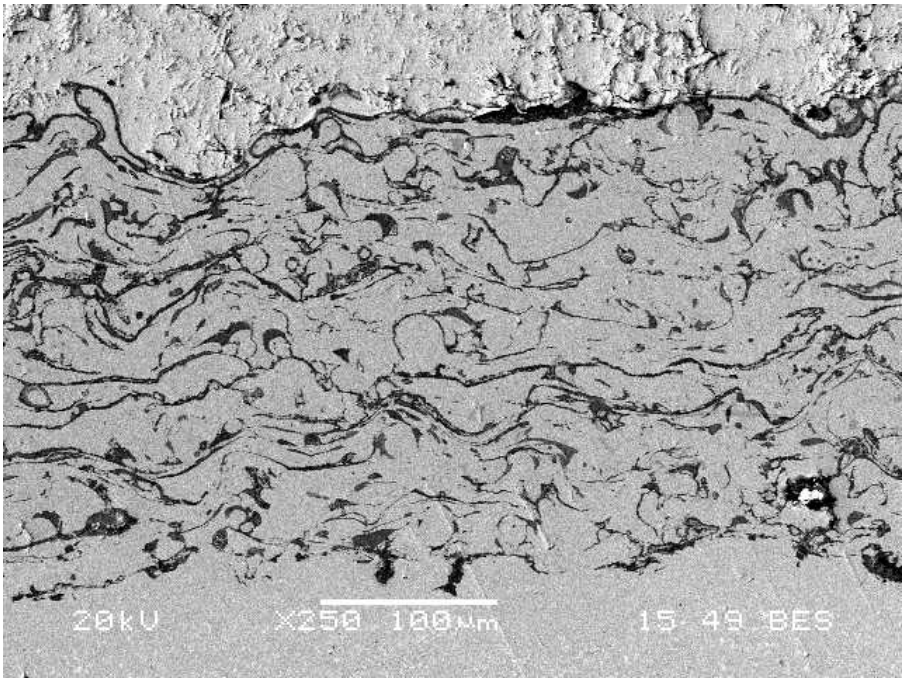

Figure 4.4.2 Back-scattered cross-sectional micrograph of specimen sprayed with salt mixture B and isothermally loaded for 700 hours at 900^{o}C.

Figures 4.4.2, 4.4.3 and 4.4.4 depict the SEM cross-section images of TBC specimen sprayed with salt mixture B (Na_2SO_4 + NaCl) and isothermally loaded for 700 hours at 900^{o}C. These three SEM micrographs were taken from the same sample and they show different localized conditions of the same specimen. Figure 4.4.2 resembles Figure 4.4.1 showing Al_2O_3 TGO layer at the interface and no cracking at the interface. However Figure 4.4.3 shows the formation of Cr-rich oxide layer near the top coat/ bond coat

interface. EDS analysis performed for this Cr-rich oxide layer is presented in Table 4.3 which shows the high percentage of Cr and O.

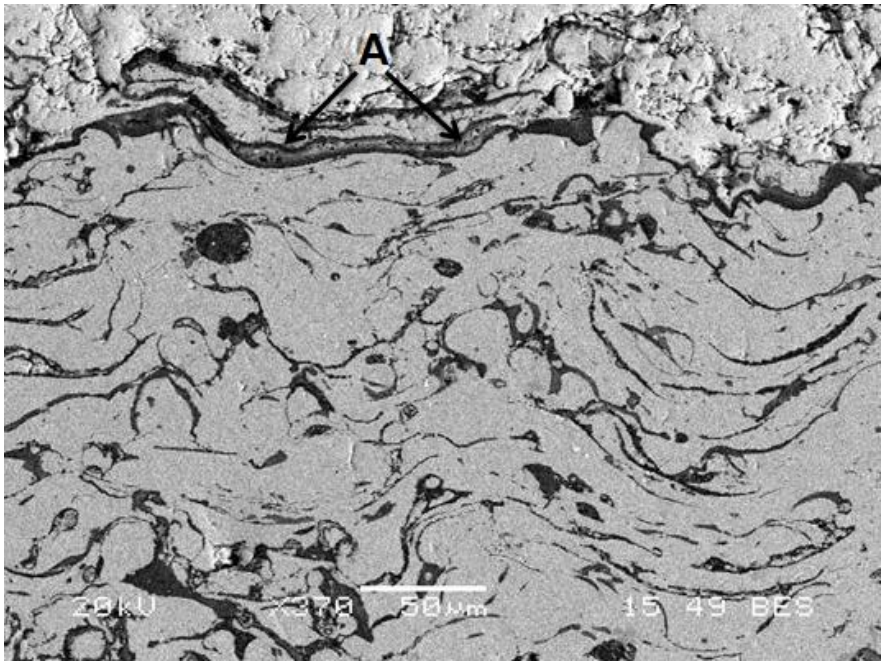

Figure 4.4.3 Back-scattered SEM Cross-section image of salt mixture B specimen after 700 hours at 900^{o}C showing initial growth of Cr-rich oxide at the top coat/bond coat interface.

Table 4.3: EDS analysis of point A in Fig 4.4.3

Point	O	Al	Cr	Ni	Y	Zr	Total
A	20.02	0	75.28	4.7	0	0	100

Figure 4.4.4 shows the SEM micrograph of specimen isothermally loaded for 700 hours at 900^{o}C showing the crack at the top coat/ bond coat interface. This specimen demonstrated the localized growth of Cr-rich oxide and also localized interfacial cracking.

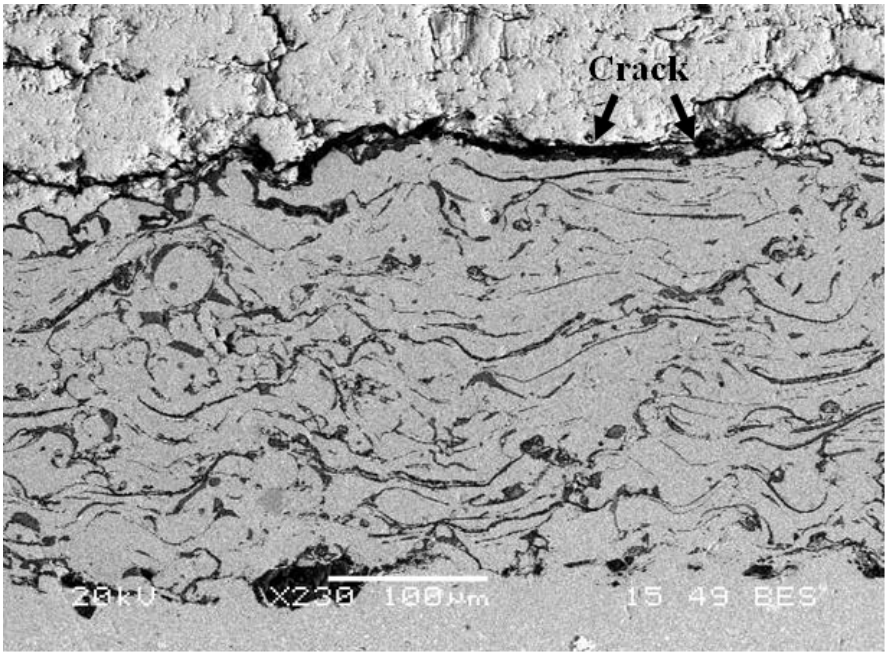

Figure 4.4.4 Back-scattered SEM Cross-section image of salt mixture B specimen after 700 hours at 900^{o}C showing interfacial cracking at the top coat/bond coat interface.

It is observed that Cr-rich oxide layer was started to form after isothermal loading for 700 hours and crack nucleation at the interface was also observed in this specimen as indicated in Figure 4.4.4.

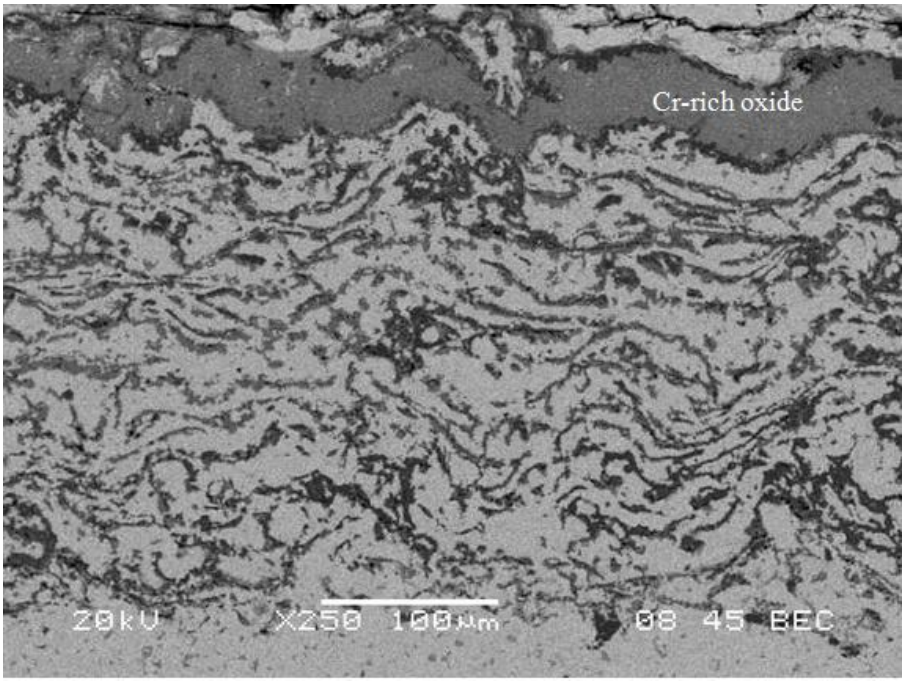

Figure 4.4.5 Back-scattered SEM Cross-section image of salt mixture B specimen after 1000 hours at 900^{o}C showing Cr-rich oxide layer.

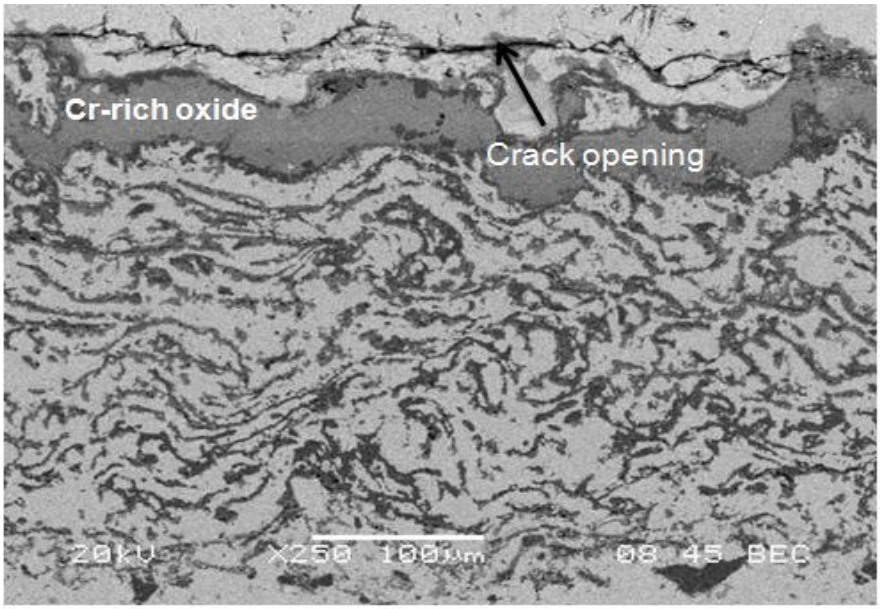

Figure 4.4.6 Back-scattered SEM Cross-section image of salt mixture B specimen after 1000 hours at 900^{o}C showing Cr-rich oxide layer and crack in top coat.

Figures 4.4.5 and 4.4.6 show SEM micrographs of the specimen sprayed with salt mixture B and loaded isothermally for 1000 hours at 900^{o}C. A prominent and thick (approximately 50µm thick) Cr-rich oxide layer was observed in this specimen after 1000 hours of isothermal exposure at 900^{o}C. The thermally grown oxide (TGO) layer was Cr-rich oxide rather than an Al_2O_3. Tables 4.4 and 4.5 illustrate the EDS analysis of such specimen. EDS analysis shows the formation of thick Cr-rich oxide layer that is uniform throughout the length of top coat/ bond coat interface. Also continuous long cracks can be seen in the ceramic top coat in Figures 4.4.6 and 4.4.7.

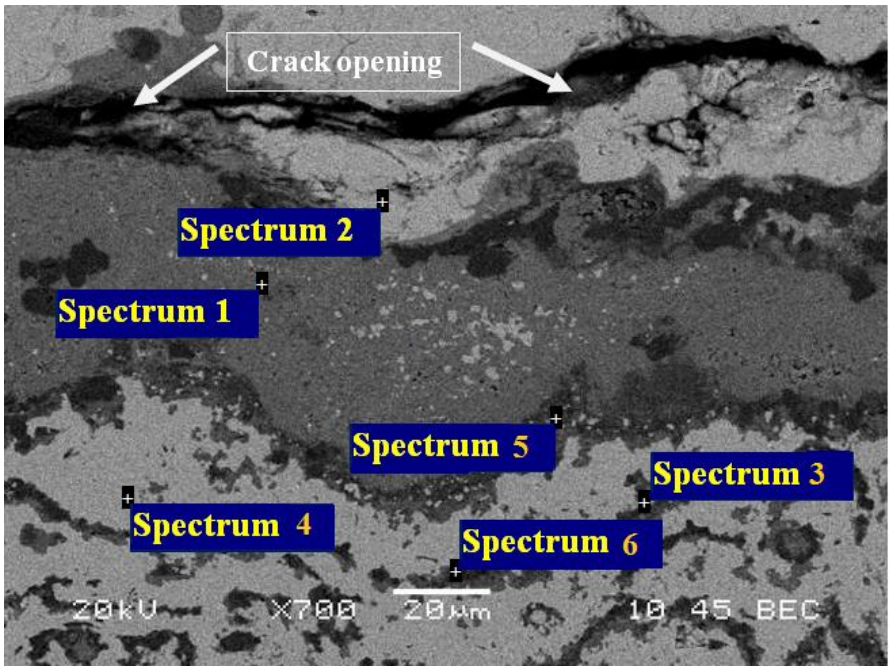

Figure 4.4.7 Back-scattered SEM image at higher magnification of salt mixture B specimen after 1000 hours at 900^{o}C and EDS analysis at points shown in Table 4.4.

Table 4.4 EDS analysis of points 1-6 in Fig. 4.3.7

Point	O	Al	Cr	Ni	Y	Zr	Total
1	18.25	0	79.08	2.67	0	0	100
2	19.27	0	0	0	5.41	75.32	100
3	39.72	49.32	0.6	10.29	0	0	100
4	0	0	16.55	83.45	0	0	100
5	30.01	50.03	15.59	4.37	0	0	100
6	36.73	57.68	1.07	10.52	0	0	100

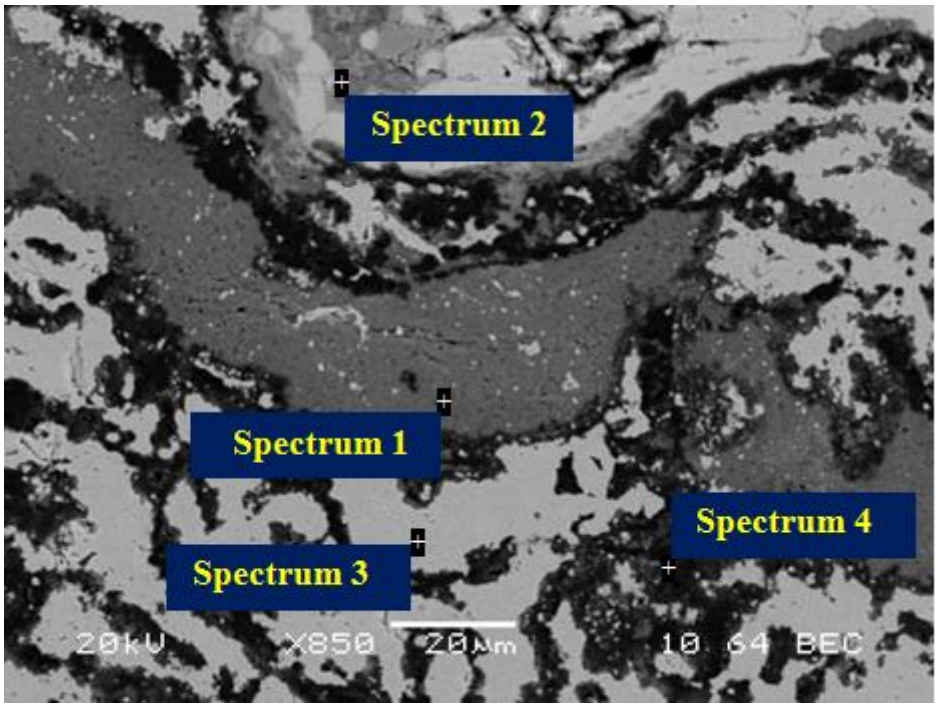

Figure 4.4.8 Back-scattered SEM image at X850 of salt mixture B specimen after 1000 hours at 900^{o}C and EDS analysis at points shown in Table 4.5.

Table 4.5 EDS analysis of points 1-4 in Fig. 4.3.8

Point	O	Al	Cr	Ni	Y	Zr	Total
1	18.61	0	78.60	3.79	0	0	100
2	20.63	0	0	0	7.48	71.89	100
3	0	0	21.71	78.29	0	0	100
4	33.08	54.48	10.52	1.92	0	0	100

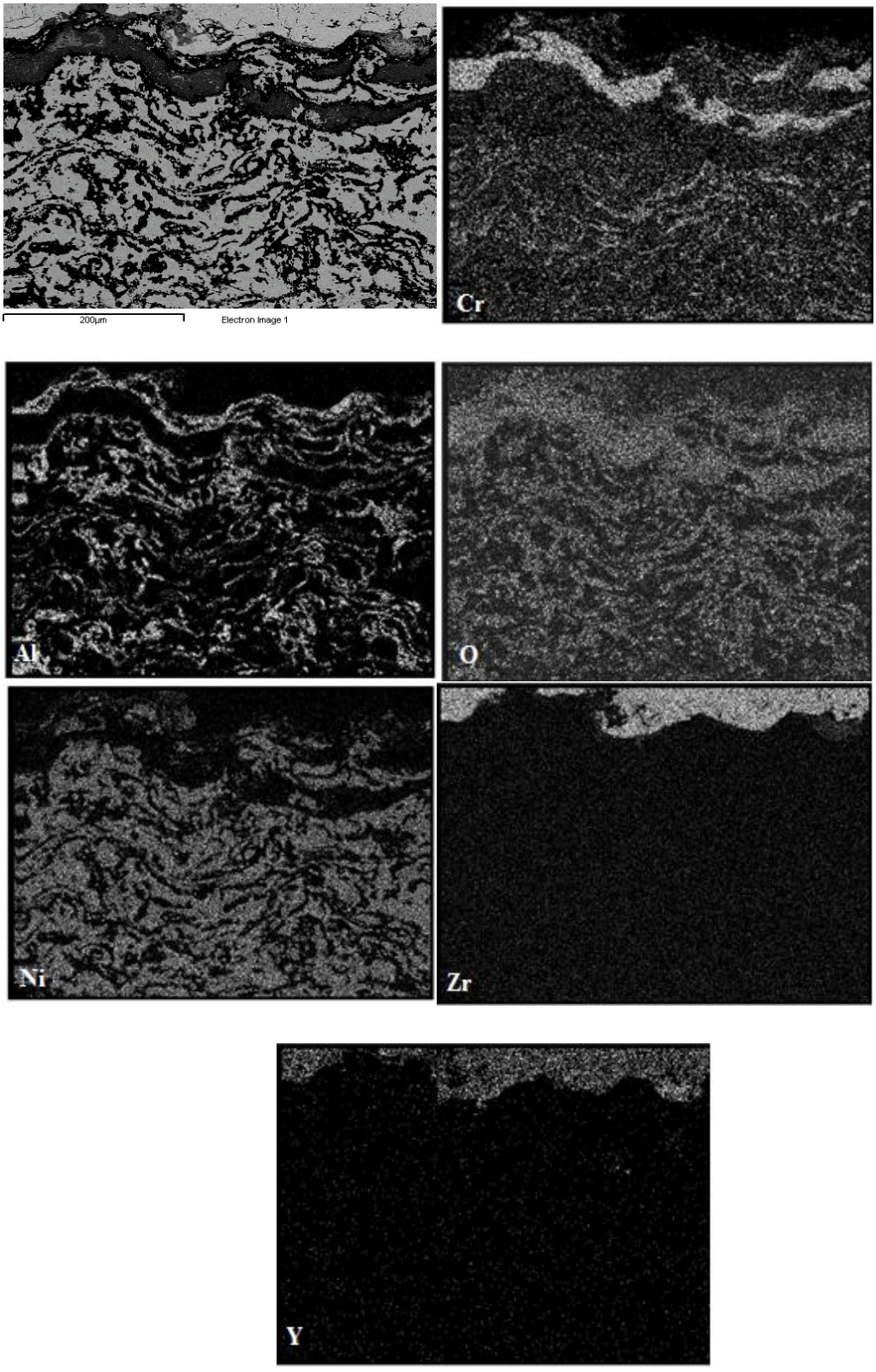

Figure 4.4.9 X-ray mapping of isothermally loaded specimen for 1000 hours at 900^{o}C sprayed with salt mixture B.

Figures 4.4.9 and 4.4.10 exhibit the elemental distribution of two different areas across the top coat/ bond coat interface of the same specimen after 1000 hours exposure. Both figures show the higher concentration of Cr near the interface as compared to the concentration of Cr at the bond coat.

Another experiment was carried out with the same experimental parameters to confirm the formation of Cr-rich oxide layer. Figure 4.4.11 shows the SEM cross-section image of specimen taken after 1100 hours of isothermal exposure and it shows the formation of Cr-rich oxide layer at the interface. Figure 4.4.12 presents the X-ray mapping of the specimen exposed for 1100 hours, showing the Cr-rich oxide formed at the interface. Figures 4.4.13 (a) and (b) demonstrate the SEM cross-section images after 1200 hours of exposure at $900^{o}C$ showing cracking at the interface and delamination of the top coat. Figure 4.4.14 shows the X-ray mapping of the still intact localized-area of the specimen exposed for 1200 hours, showing the Cr-rich oxide formed at the interface. This specimen is considered as a total failure as the ceramic top coat is spalled off and the top coat can no more be utilized for its intended use as a thermal barrier. The majority of the interface length has developed cracks because of the formation of thick Cr-rich oxide layer.

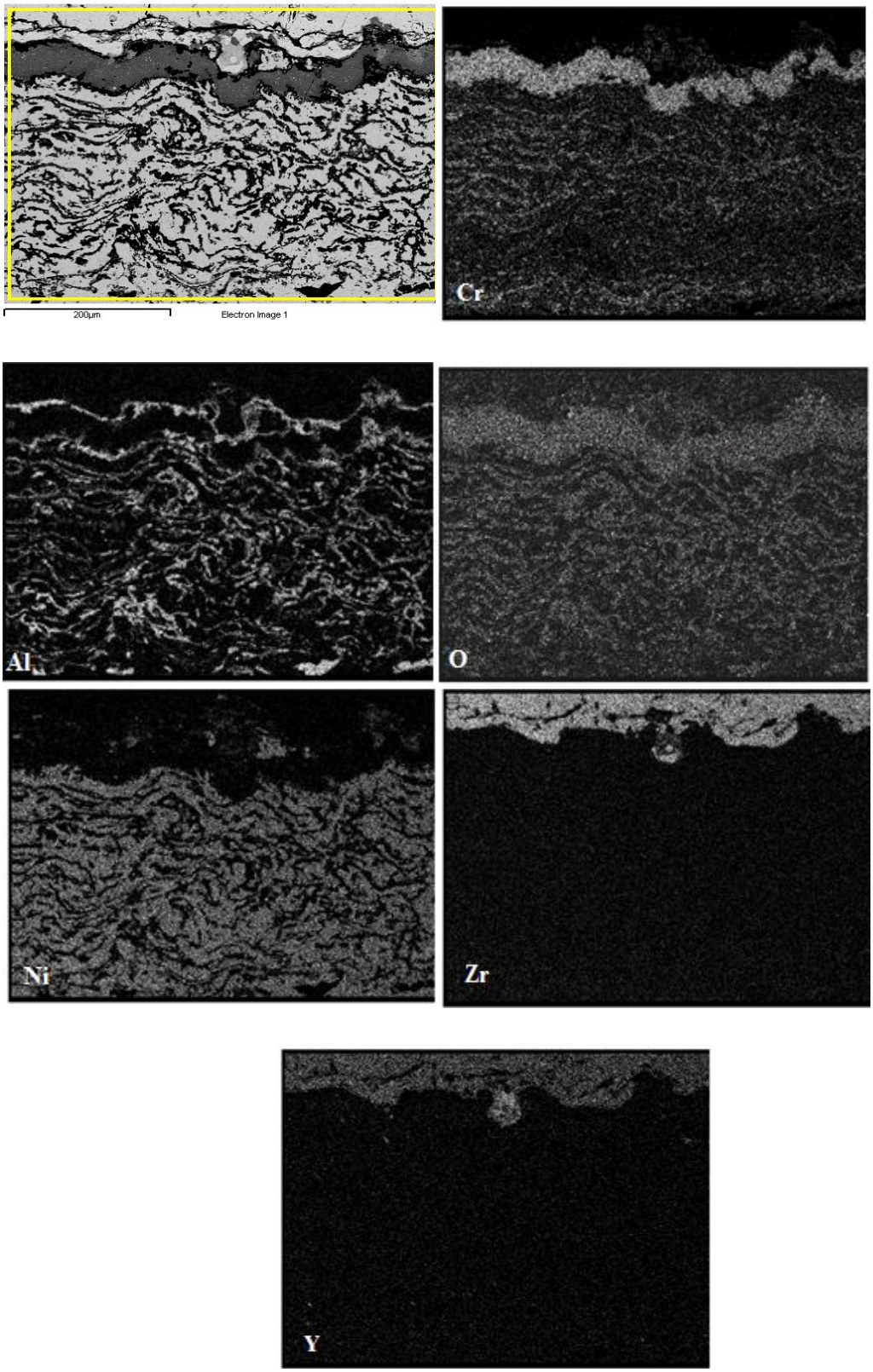

Figure 4.4.10 Elemental distribution of isothermally loaded mixture B coated specimen for 1000 hours at 900^{o}C.

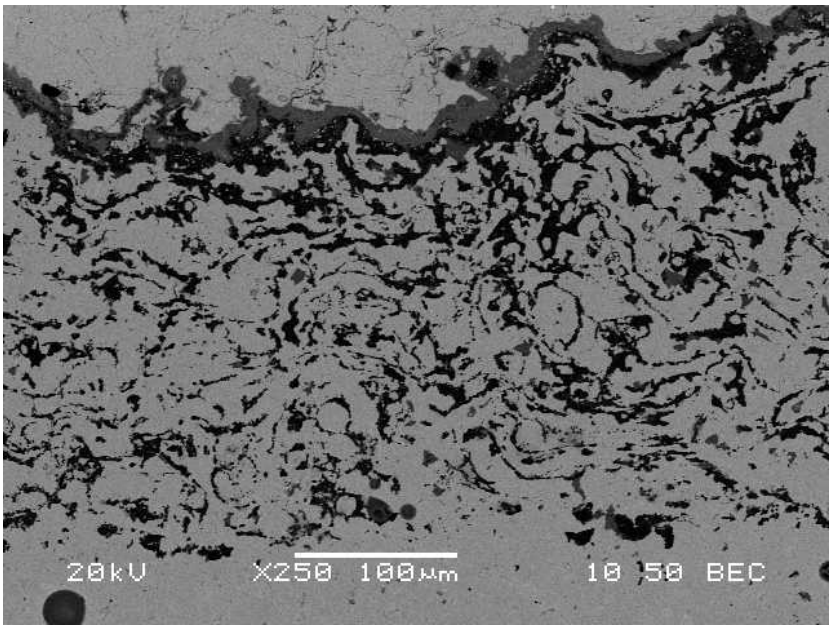

Figure 4.4.11 Back-scattered SEM Cross-section image of specimen after 1100 hours at 900^{o}C showing Cr-rich oxide layer.

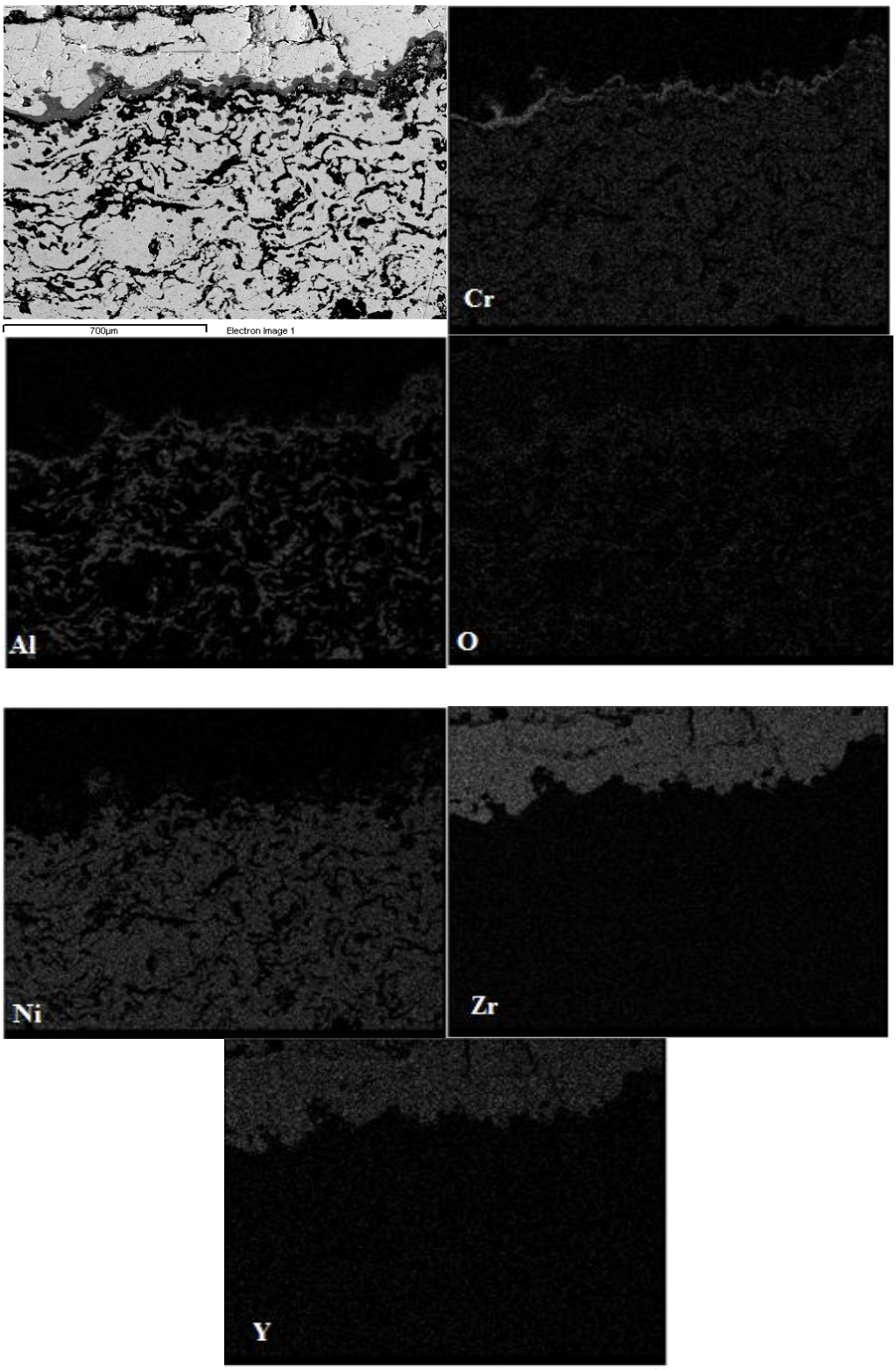

Figure 4.4.12 Elemental distribution of isothermally loaded mixture B coated specimen for 1100 hours at 900^{o}C.

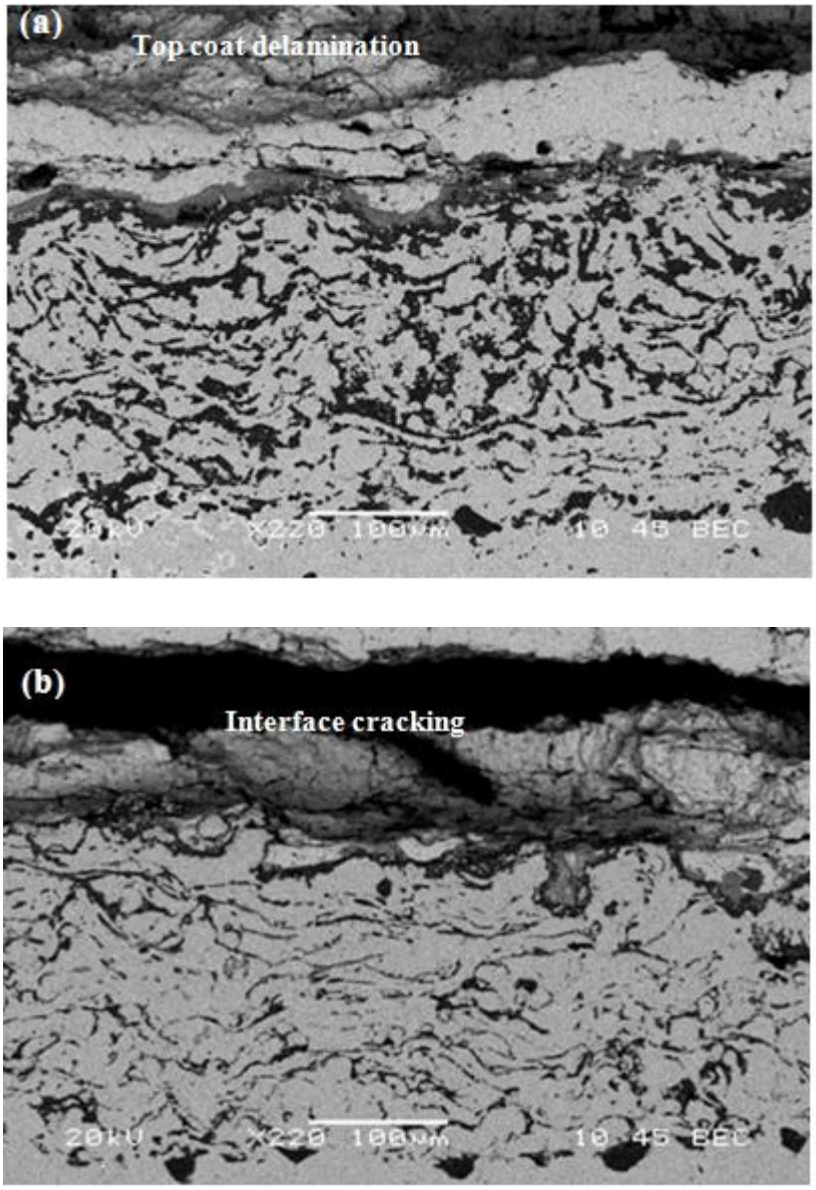

Figure 4.4.13 Back-scattered SEM Cross-section images (a) and (b) of specimen after 1200 hours at 900^{o}C.

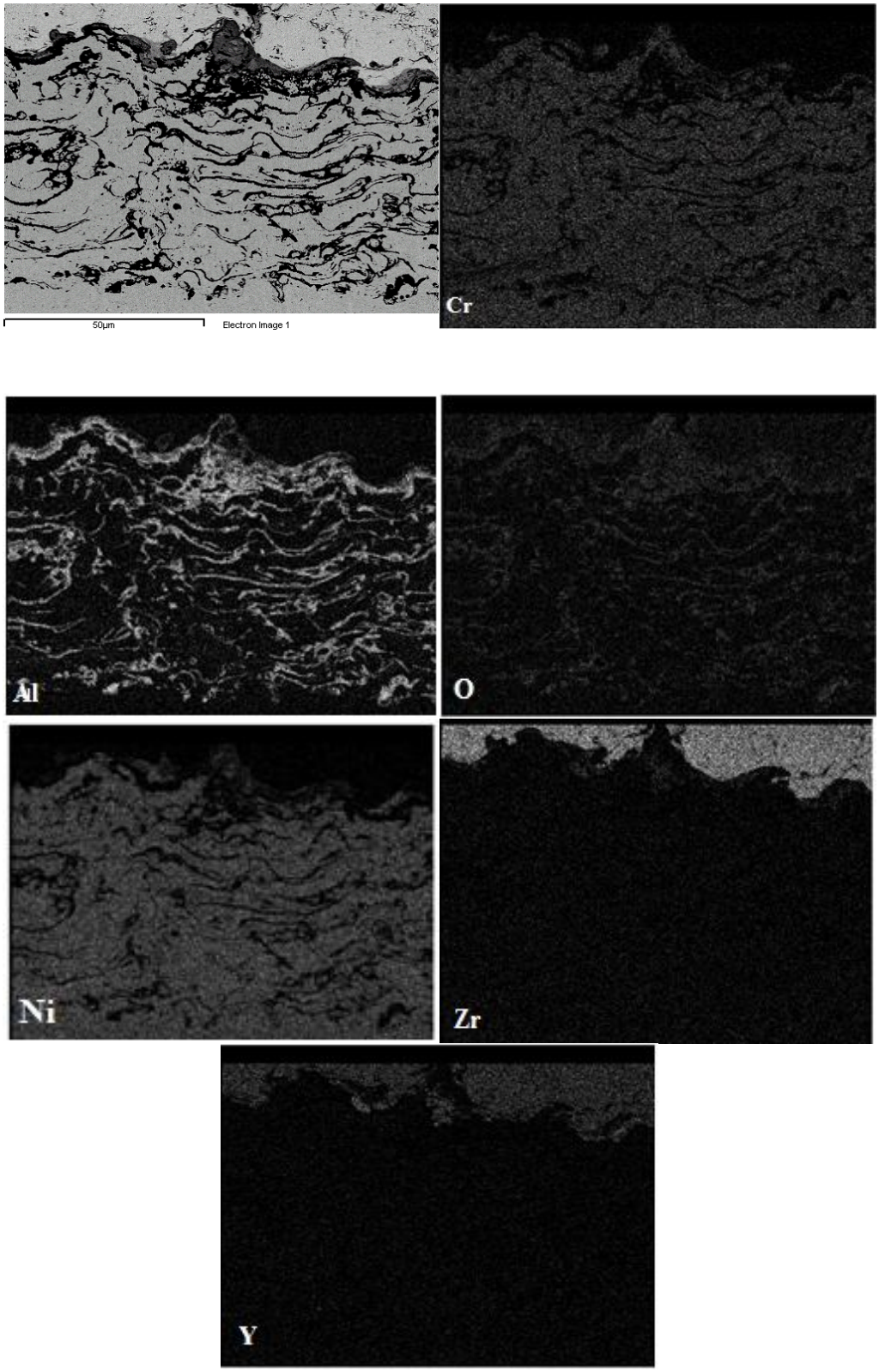

Figure 4.4.14 Elemental distribution of isothermally loaded mixture B coated specimen for 1200 hours at 900^{o}C.

CHAPTER 5 DISCUSSION

5.1 Degradation in Purely Oxidizing Environment

TBC specimens were exposed isothermally up to 1200 hours at 900^{o}C to study the effect of oxidation without presence of impurity salts. The TBC specimens showed a progressive thickening of protective Al_2O_3 TGO layer with increase of exposure time from 400 hours to 1200 hours as can be seen in Figures 4.2.1-4.2.3 and 4.2.5. Figure 4.2.5 shows the X-ray mapping of specimen exposed for 1200 hours indicating a thick alumina TGO at the interface developed due to growth of Al_2O_3 layer at the interface. The thick Al_2O_3 layer was protecting the oxidation of underneath bond coat elements. No delamination or spallation of top coat was observed in these specimens indicating the effective protection provided by Al_2O_3. Figure 5.1.1 reveals the image of TBC specimen that was exposed to 1000 hours and no damage or spallation of top coat is observed.

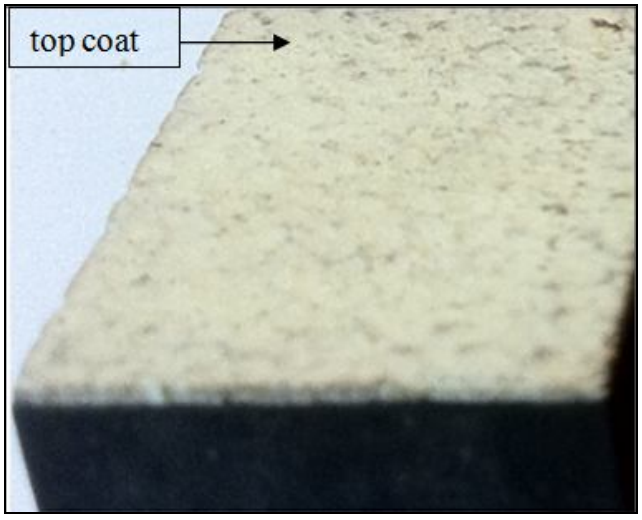

Figure 5.1.1 Image of TBC specimen after exposure for 1200 hours at 900^{o}C showing ceramic top coat intact with the substrate.

Also, slow thickening of alumina splats is observed with isothermal exposure time due to oxidation. The critical TGO thickness before mechanical failure in TBCs with typical MCrAlY bond coat has been reported in the literature to be 6–9 μm [51, 52]. In the present study the TGO thickness after isothermal exposure for 1200 hours is approximately 4-6 μm and no interface damage was observed until 1200 hours. This suggests that, under pure oxidation environment, TBC can sustain beyond 1200 hours of exposure without TGO developing cracks at the interface and failing due to mechanical damage.

5.2 Degradation in Salt Mixture A ($Na_2SO_4 + V_2O_5$)

Figure 4.1.2 shows the XRD pattern of the as received specimen showing only the peaks for tetragonal zirconia in the top coat. This XRD pattern shows only tetragonal zirconia with no evidence of monoclinic phase or YVO_4.

Figure 4.3.4 shows the XRD pattern in which it is evident that tranformation of tetragonal zirconia to monoclinic phase took place in the specimen that was isothermally loaded for 400 hours in salt A. This transformation is accompanied by 3–5% volume expansion, leading to interface cracking as shown in Figure 4.3.2 and delamination of top coat as shown in Figure 4.3.3. This phase transformation started after 400 hours and resulted in complete failure after 700 hours at 900^{o}C. Rod like YVO_4 particles were formed on the surface as shown in Figure 4.3.5 and 4.3.6. These particles grew outward of surface and resulted in further development of stresses in the coating which caused formation of cracks in YSZ top coat [53].

V_2O_5 and Na_2SO_4 react to form $NaVO_3$ at the surface of top coat. $NaVO_3$ acts as a leaching agent for yttria, the stabilizer of zirconia, which results in the transformation of tetragonal zirconia to monoclinic phase. The phase diagram of stabilized YSZ is shown in Figure 2.2.3.

The mechanism can be explained by the following reactions [25, 26];

$$V_2O_5 + Na_2SO_4 \rightarrow 2NaVO_3 + SO_3 \qquad (5.2.1)$$

$$ZrO_2\,(Y_2O_3)\ (\text{tetragonal}) + 2NaVO_3 \rightarrow ZrO_2\ (\text{monoclinic}) + 2YVO_4 + Na_2O \qquad (5.2.2)$$

5.3 Degradation in Salt Mixture B (Na_2SO_4 + NaCl)

The free energy change of a reaction in terms of the partial pressure of the oxygen gas is written as [54]:

$$\Delta G = \Delta G^{o} - RT \ln P_{O2} \quad (5.3.1)$$

The partial pressure of oxygen in the present study is the atmospheric partial pressure for oxygen (P_{O2} = 0.02 MPa). Figure 5.3.1 illustrates variation in free energies of oxide formation with respect to temperatures at P_{O2}= 0.02 MPa. The diagram reveals that at 900^{o}C (1173.15 K), Al_2O_3 has most negative free energy of formation i.e. it is most favorable to form, followed by Cr_2O_3. The ΔG^{o} values for Al_2O_3 and Cr_2O_3 at different temperatures are obtained from NIST-JANAF Thermochemical Tables.

Ideally it is desirable that a continuous alumina layer is formed in the TGO which acts as an oxygen diffusion barrier to suppress the formation of other detrimental oxides during high temperature exposure for longer times. This protects the underneath substrate from oxidation and improve the durability of the TBC system.

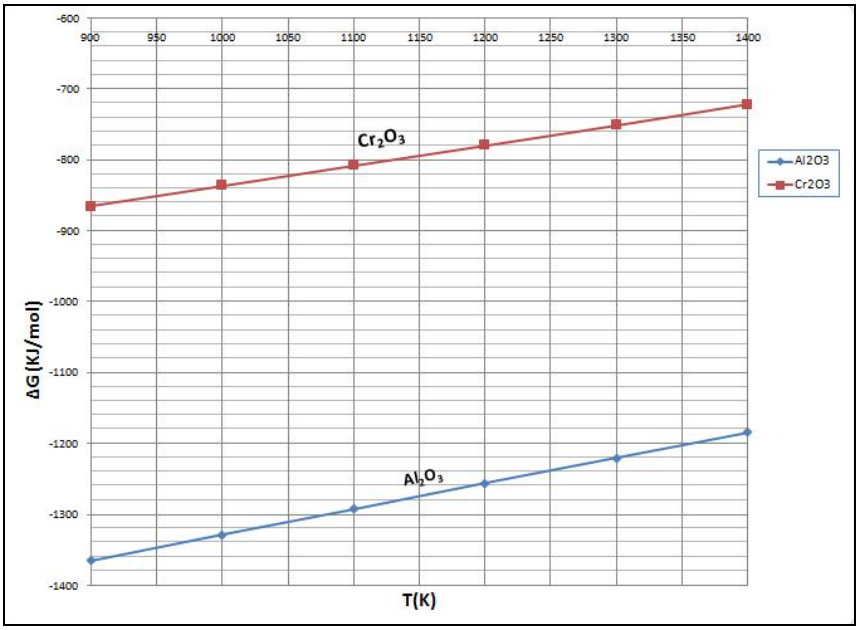

Figure 5.3.1 ΔG Vs T(K) plot for the three different oxide reactions

Figure 4.3.3 shows the initiation of formation of Cr-rich oxide layer at the top coat and bond coat interface after 700 hours of isothermal exposure and thickness of this Cr- rich oxide layer increased after 1000 hours of isothermal exposure as shown in Figures 4.3.5 and 4.3.6. The initiation of this Cr-rich oxide layer is attributed to the role of Na_2SO_4 and NaCl in damaging the stable Al_2O_3 TGO as explained using equations 5.3.2-5.3.4 later in this section. The growth of this Cr-rich oxide layer was also observed when experiment was repeated for 1100 hours of isothermal exposure. The growth of Cr-rich oxide layer at the interface caused cracking at the interface and in the top coat. In light of aforementioned results in Chapter 4 section 4.3, it is suggested that TBC specimens have experienced accelerated oxidation when their surfaces were covered with thin film of saturated salt mixture B (75% Na_2SO_4 + 25% NaCl) and exposed at elevated temperature at 900^{o}C.

The YSZ top coat condition after 1000 hours of isothermal can be observed in Figure 5.3.2 depicting the spallatation of top coat from some areas exposing the bare bond coat to high temperature. Another set of specimens with two different salt compositions namely, 75% Na_2SO_4 and 25 % NaCl, was also exposed at 900^oC for 1000 hours to investigate the effect of these impurity salts on top coat when sprayed separately rather than in the form of a mixture i.e. 75% Na_2SO_4 + 25% NaCl. The characterization results revealed that there was no spallation or delamination of topcoat when salts were sprayed separately on TBC specimens as can be observed in Figures 5.3.2-5.3.6.

X-ray mapping of 25% NaCl sprayed specimen is illustrated in Figure 5.3.7 showing absence of Cr-rich oxide TGO at the interface and Figure 5.3.8 depicts the same conclusion for TBC specimen sprayed with 75% Na_2SO_4. Therefore it is concluded that a Cr-rich oxide layer at interface forms only when TBC specimens are sprayed with a mixture of 75% Na_2SO_4 + 20% NaCl.

The molten salt mixture B contains Na_2SO_4 which melts at 884^oC but when NaCl is added its melting point is lowered. It is dissociated by the following reaction [55]:

$$Na_2SO_4\ (l) \rightarrow Na_2O\ (l) + SO_3\ (g) \qquad (5.3.2)$$

Na_2O penetrates through the pores of ceramic top coat to reach the top coat/ bond coat interface. Na_2O reacts with Al_2O_3 TGO resulting in the following basic fluxing reaction:

$$Al_2O_3 + Na_2O + O_2 \rightarrow 2NaAlO_2 \qquad (5.3.3)$$

Also, in the molten salt mixture of Na_2SO_4 and NaCl, it is possible that Al_2O_3 TGO reacts with NaCl by the following reaction [56-58]

$$2NaCl + Al_2O_3 + ½\ O = 2NaAlO_2 + Cl_2 \quad (5.3.4)$$

Sodium aluminate ($NaAlO_2$) is metastable phase allowing oxygen to diffuse in and react with Cr to form a Cr-rich oxide at the interface. It is suspected that the presence of NaCl in salt mixture accelerates the formation of $NaAlO_2$, basic fluxing and thus Cr-rich oxide formation as no Cr-rich oxide was observed when Na_2SO_4 solution was used without NaCl. The formation of Cr-rich oxide layer is also attributed to the aluminum depletion in the bond coat. The amount of aluminum level in the bond coat is dropped below the level at which protective alumina TGO can form and therefore protective alumina scale is not formed preferentially. This leads to a faster interaction between the corrosive species present on the surface of TBC and the non-protective oxides of other elements of the bond coat. Fig.4.1.1 shows the SEM image of the as-received TBC specimen and Table 4.1 shows the EDS analysis of this specimen. Figures 4.4.7, 4.4.8 and Tables 4.4 and 4.5 show the SEM images and EDS analysis of the specimen showing Cr-rich oxide layer after 1000 hours of isothermal exposure at 900^{o}C. It is evident from the EDS comparison of as-received specimen (Figure 4.1.1) with the specimen showing Cr-rich rich oxide layer (Figures 4.4.7 and 4.4.8) that the amount of aluminum in bond coat has decreased when exposed for extended time at the higher temperature. More and more aluminum is being consumed in the thickening of alumina splats in the bond coat.

However, Figure 4.2.5 (elemental distribution of pure-oxidation specimen exposed isothermally for 1200 hours at 900^{o}C.) shows the higher concentration of Cr and Ni in the bond coat similar to the as-received condition shown in Figure 4.1.3 in contrast to Cr-rich oxide near the interface.

Figure 5.3.2 Image of TBC specimen sprayed with salt mixture B and exposed for 1000 hours at 900^{o}C showing spalling of ceramic top.

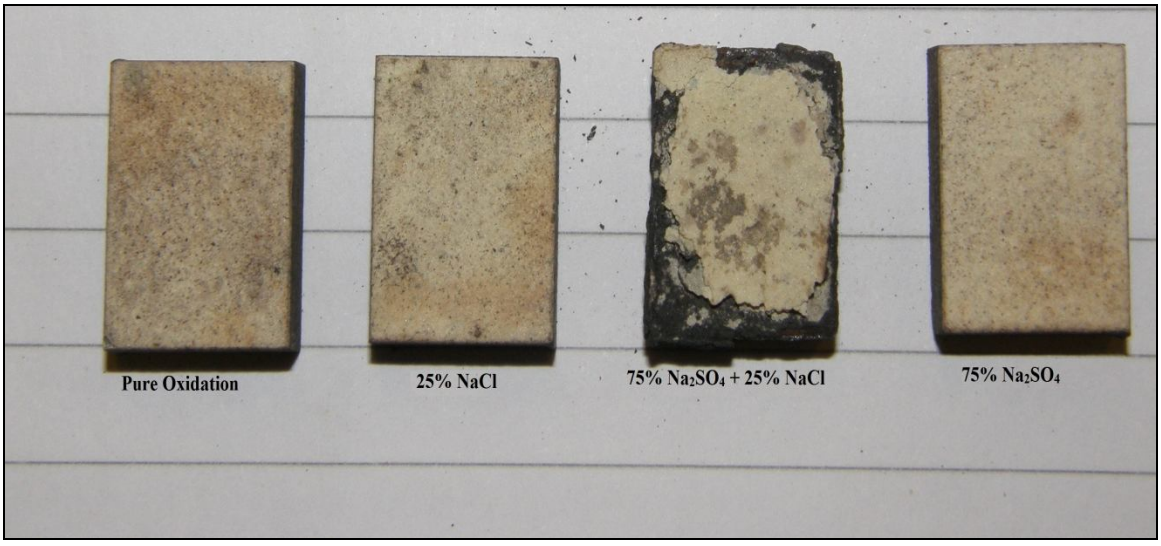

Figure 5.3.3 Top view of four different TBC specimens exposed isothermally for 1000 hours at 900^{o}C.

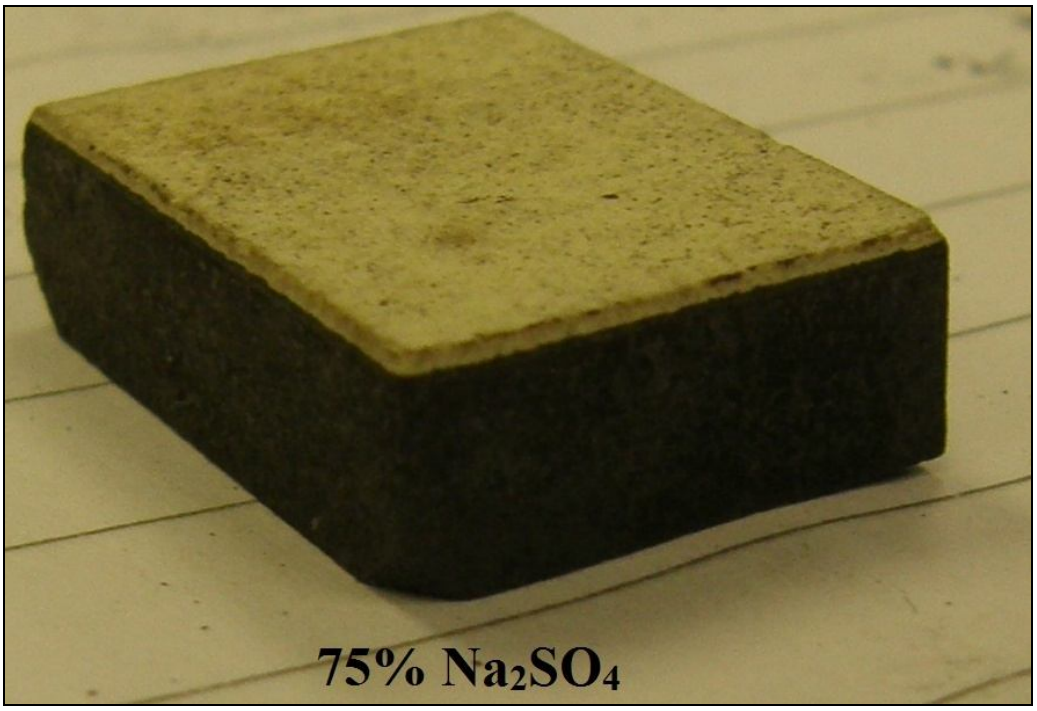

Figure 5.3.4 TBC specimen sprayed with 75% Na_2SO_4 and exposed isothermally for 1000 hours at 900^oC.

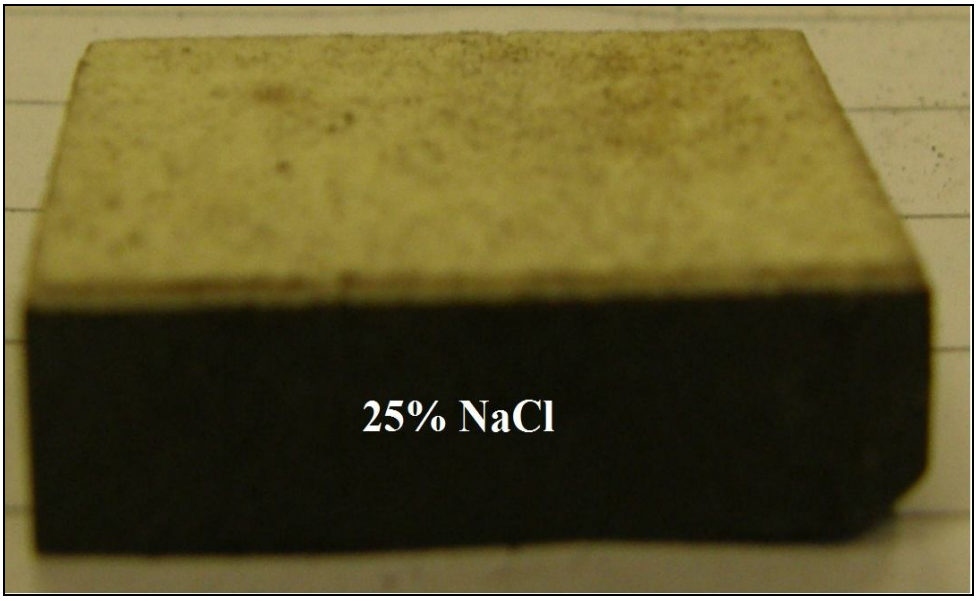

Figure 5.3.5 TBC specimen sprayed with 25% NaCl and exposed isothermally for 1000 hours at 900^{o}C.

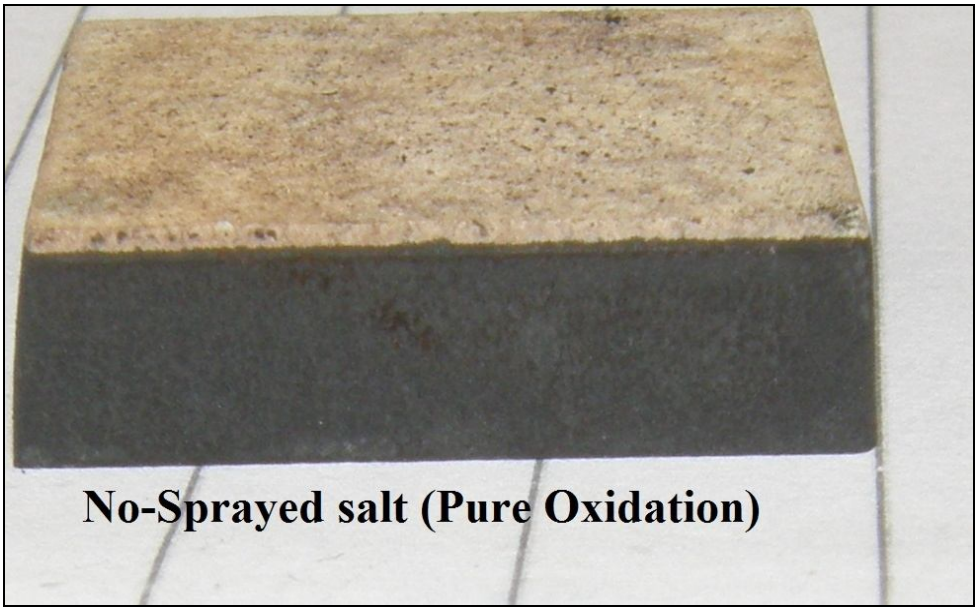

Figure 5.3.6 Pure oxidation TBC specimen exposed isothermally for 1000 hours at 900^{o}C.

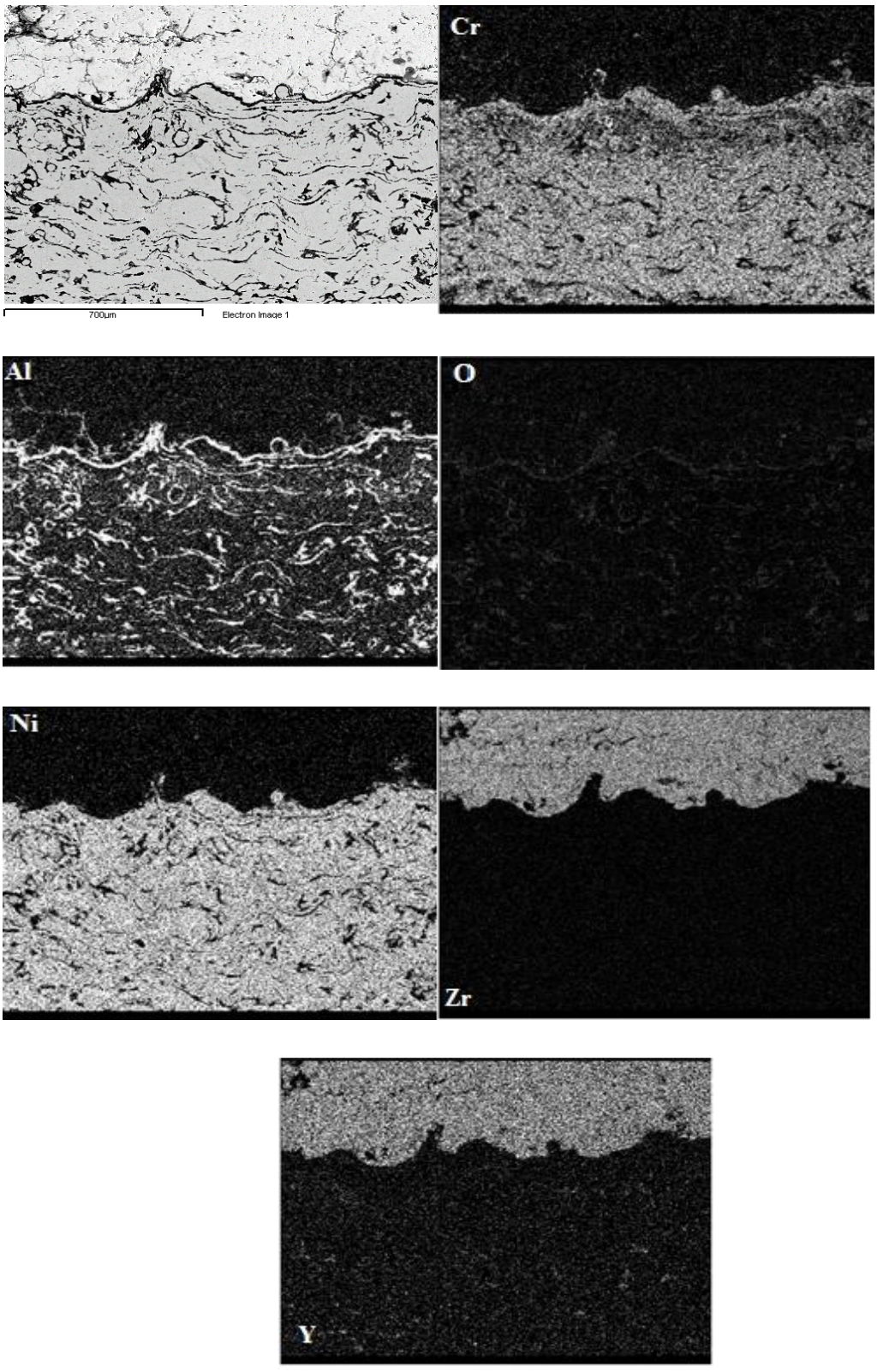

Figure 5.3.7 X-ray mapping of TBC specimen sprayed with 25% NaCl and exposed for 1000 hours at 900^{o}C

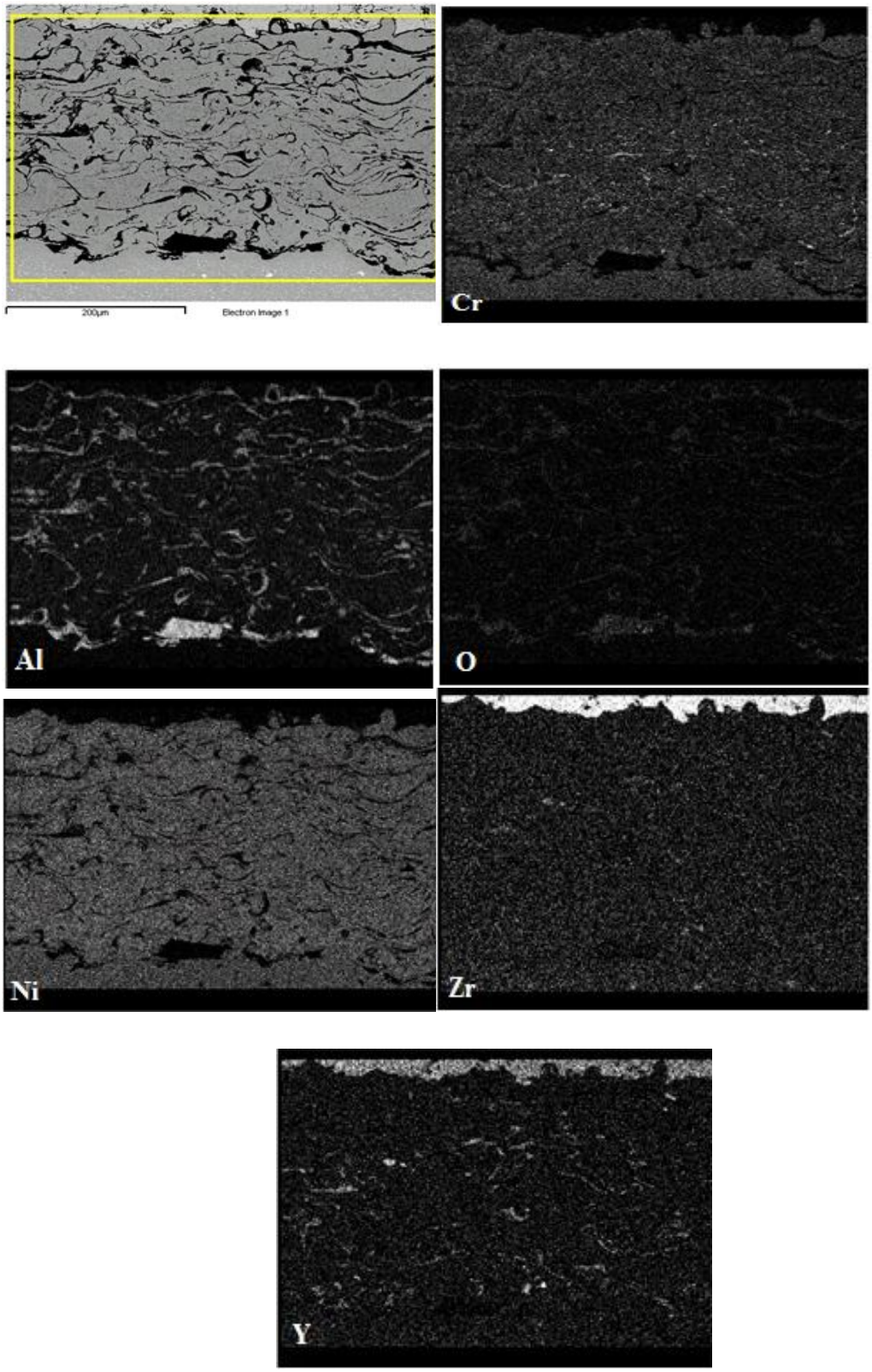

Figure 5.3.8 X-ray mapping of TBC specimen sprayed with 75% Na_2SO_4 and exposed for 1000 hours at 900^oC

Crack nucleation, propagation and delamination of TBC was found to be associated with the formation of Cr-rich oxide layer because after isothermally loading for 1200 hours at 900^{o}C top coat was completely spalled off as shown in Figure 4.4.13 (a) and (b).

Due to the formation of Cr-rich oxide layer at the interface, there is an increase in the volume change due to the formation of the oxide as predicted by the Pilling-Bedworth ratio (PBR) [59].

PBR= Volume of oxide/ Volume of metal

This increase in volume results in increase of stresses in the ceramic top coat near the interface which can cause the already present small cracks to join and grow. Table 5.1 demonstrates higher PBR value of Cr-oxide as compared to aluminum oxide, nickel oxide, and Yttrium oxide.

Table 5.1 Values of Pilling-Bedworth ratios for different oxides [60].

Metal	**Metal Oxide**	**PBR**
Chromium	Chromium Oxide	2.07
Aluminum	Aluminum Oxide	1.28
Nickel	Nickel Oxide	1.65
Yttrium	Yttrium oxide	1.56

Moreover, the fracture mechanisms observed in APS and EB-PVD systems have in common that the delamination is predominantly located in an essentially brittle ceramic material or along the interfaces between brittle ceramics. The fracture of ceramic materials is conveniently described in terms of fracture energy or fracture toughness.

Thus inherent micro cracks present in the top coat, under the influence of Cr-rich oxide layer formation after extended isothermal exposure, coalesce and result in the spallation of ceramic top coat layer. Once the protective ceramic top coat layer is removed the TBC coated superalloy is no longer suitable for higher temperature insulation.

CHAPTER 6 CONCLUSIONS

The conclusions of this study are summarized below:

1. No damage to the bond coat or top coat was observed in specimens exposed to air for 1200 hours of isothermal exposure at 900^{o}C. However, slow thickening of Al_2O_3 TGO layer was observed in these specimens.
2. Transformation of tetragonal zirconia to monoclinic phase was observed after 400 hours of exposure in specimens sprayed with salt mixture A ($Na_2SO_4 + V_2O_5$) and this transformation resulted in spallation of top coat after 700 hours at 900^{o}C.
3. No detectable damage in the bond coat was observed in salt mixture A specimens for up to 700 hours of exposure at 900^{o}C and thermally grown oxide (TGO) layer at the interface was Al_2O_3 until failure.
4. TBC specimens sprayed with salt mixture B (Na_2SO_4 + NaCl) completely failed due to spallation of top coat after 1000 hours of isothermal loading at 900^{o}C.
5. Cr-rich oxide layer started to form near the top/bond coat interface in specimens sprayed with salt mixture B after 700 hours of exposure at 900^{o}C. The oxide layer grew in thickness with longer exposure time and resulted in delamination of top coat after 1000 hours of exposure.
6. The formation of Cr-rich oxide was attributed to fluxing of the protective TGO (Al_2O_3) and depletion of free Al near the top/bond coat interface.
7. No Cr-rich oxide layer was observed in specimens sprayed with 75% Na_2SO_4 or in specimens sprayed with 25% NaCl and isothermally exposed to 900°C for up to 1000 hours.

REFERENCES

1. Strangman, T.E. Development and Performance of Physical Vapour Deposition Thermal Barrier Coatings Systems. Paper presented at the 1987 Workshop on Coatings for Advanced Heat Engines, Castine, Maine 1987.
2. Tolpygo, V.K., D.R. Clarke, K.S. Murphy. Surface and Coatings Technology, 2001. 146-147: p. 124-131.
3. V.K. Tolpygo. Surface and Coatings Technology, 1999. 120-121: p. 53-60.
4. Padture, Nitin P.; Gell, Maurice; Jordan, Eric H. Science, 2002. 296: p.280.
5. A. Maricocchi, A. Barz, and D. Wortman, PVD TBC Experience on GE Aircraft Engines, Thermal Barrier Coating Workshop, NASA Lewis Research Center, Cleveland, OH, March 27-29, NASA Conference Publication, 1995. 3312: p 79-90.
6. Yasuda, K., K. Suenaga, K. Wada. Journal of Materials science, 2000. 35(2): p. 317.
7. Unal, O., T.E. Mitchell, A.H. Heuer. Journal of American Ceramic Society, 1994. 77(4): p. 984.
8. Majerus, P., New methods for analysis of deformation and damage to behavior of MCrAlY coatings in thermal barrier coating system. RWTH-Aachen. IEF-2.2003: p. 157.
9. Golightly, F.A., F.H. Stott, and G.C. Wood. Oxid. Met., 1957. 10: p. 163.
10. Meschke F, Raddatz O, Kolleck A. Journal of American Ceramic Society, 2000. 83(2): p. 353-361.
11. Scott, H.G. J. Mat. Sci., 1975. 10: p. 1527-1535.

12. Bratton, R.J. and S.K. Lau, ZrO_2 Thermal Barrier coatings. Advances in Ceramics, The American Ceramic Society, Columbus, OH, 1981. 3: p. 226-240.
13. Yasuda, K., K. Suenaga, K. Wada. Journal of Materials science, 2000. 35(2): p. 317.
14. Unal, O., T.E. Mitchell, and A.H. Heuer. Journal of American Ceramic Society, 1994. 77(4): p. 984.
15. Padture, N.P. Science, 2002. 296: p. 280-284.
16. Gell, M, K.Vaidyanathan, K. McCarron, B. Barber, Y.H. Sohn, V.K. Tolpygo. Surface and Coatings Technology, 1999. 120-121: p. 53-60.
17. Wada, K., N. Yamaguchi, H. Matsubara. Surface and Coatings Technology, 2005. 191: p. 367.
18. Schulz, U., K. Fritscher, C. Leyens. Journal of Engineering for Gas Turbines and Power, 2002. 124.
19. Schlichting, K.W., N. P. Padture, E. H. Jordan, M. Gell. Materials Science and Engineering A, 2003. 342: p. 120-130.
20. Smialek, J.L., R. Browning. Proc. Electrochem. Soc., 1986. 86: p. 258.
21. F.S Petit and G.W. Goward. Coatings for High Temperature Processes, E. Lang, Ed., Applied Science Publishers, 1985.
22. Albert Feuerstein, James Knapp, Thomas Taylor, Adil Ashary, Ann Bolcavage, Neil Hitchman. Journal of Thermal Spray Technology, 2008. 17(2).
23. R. Bouchet, R. Mevrel. Defect Diffusion Forum, 2005, 237-240: p 238-245.
24. Golightly, F.A., F.H. Stott, G.C. Wood. Oxid. Met., 1957. 10: p. 163.
25. Prescott, R. and M.J. Graham. Oxid. Met., 1992. 38: p. 233.

26. Brandl, W. Surface and Coatings Technology, 1996. 86-87: p. 41-47.

27. Golightly, F.A., F.H. Stott, G.C. Wood. Oxid. Met., 1957. 10: p. 163.

28. Pfeiffer, H., Werkst. Korros., 1957. 8: p. 575.

29. Smialek, J.L. and R. Browning. Proc. Electrochem. Soc., 1986. 86: p. 258.

30. Mennicke, C., M.-Y. He, D.R. Clarke, J.S. Smith. Acta Mater., 2000. 48: p. 2941.

31. Prescott, R. M.J. Graham. Oxid. Met., 1992. 38: p. 233.

32. Tolpygo, V.K., J.R. Dryden, D.R. Clarke. Acta Mater., 2000. 48: p. 3283.

33. Christensen, R.J., D.M. Lipkin, D.R. Clarke. Appl. Phys. Lett., 1996: p. 3754.

34. Busso, E.P., McClintock, F.A. Acta materialia, 2001. 49: p. 1515-1528.

35. Brindley, W.J, J.D. Materials Science and Engineering A, 1993. 163: p. 33-41.

36. Balmain, J., M.K. Loudjani, A.M. Huntz. Materials Science and Engineering A, 1997. 224: p. 87.

37. Monceau, D., E. Busso, G. Cailletaud. MECAMAT, Mechanics and Multiphysics Processes in Solids, 1998.

38. Garriga-Majo., B.A. Shollock, D.S. McPhail, R.J. Chater. J. Inorg. Mater., 1999. 1: p. 325.

39. A.G.Evans, J.S. Wang, D.Mum. Mechanism-Based Life Prediction Issues for Thermal Barrier Coatings. TBC Workshop, Cincinnati, Ohio, 1997.

40. B. Pint., I. Wright, W. Lee, Y. Zhang, Substrate and Bond Coat compositions: Factors affecting Alumina Scale Adhesion. TBC Workshop, Cincinnati, Ohio, 1997.

41. A.G. Evans, D.R. Mumm, J.W. Hutchinson, G.H. Meier, F.S. Pettit. Prog. Mater. Sci., 2001.46: p.505.

42. C.Batista, A. Portinha, R.M. Ribeiro,V. Teixeira, C.R. Oliveira. Surf. Coat. Technol., 2006.200: p. 6783.
43. H.C. Chen, Z.Y. Liu, Y.C. Chuang. Thin Solid Films, 1992.223: p. 56.
44. S.Y. Park, J.H. Kim, M.C. kim, H.S. Song, C.G. Park. Surf. Coat. Technol., 2005.190: p. 357.
45. A. Afrasiabi. Materials Science and Engineering A, 2008.478: p 264–269.
46. S. Alperine, M. Derrien, Y. Jaslier, and R. Mevrel, Thermal Barrier Coatings-The Thermal Conductivity Challenge, AGARD Report 823 ‘‘Thermal Barrier Coatings,’’ 15-16 October 1997: p. 1.1-1.10.
47. A. Feuerstein, A. Bolcavage, Thermal Conductivity of Plasma and EBPVD Thermal Barrier Coatings, Proceedings ASM International Surface Engineering Congress 2004, Orlando, Florida.
48. N.S. Bornstein. JOM 48, 1996. 37-39.
49. E. P. Busso, F. A. McClintock, Thermal fatigue degradation of an overlay coating. Mat. Sci. Eng., 1992. A161: p. 165-179.
50. Helble, J.J., Mojtahed W, Lyyriinen J, Jokiniemi J, Kauppinen E. Fuel, 1996. 75(8): p. 931–939.
51. V.K. Tolpygo. Surface and Coatings Technology, 2001.146-147: p. 124–131.
52. T. Tomimatsu., S. Zhu, Y. Kagawa. Acta Materialia, 2003.51: p. 2397–2405.
53. Zhang, X.C. Applied Surface Science, 2008. 254: p. 1881–1889.
54. A.S. Khanna, High Temperature Oxidation and Corrosion, ASM International, OH, 2002.
55. R.A. Rapp, Y.S. Zhang. JOM, 1994.46: p 47-55.

56. Zhaolin Tang, Fuhui Wang, Weaitao WU. Oxid. Met., 1999: p. 235.

57. N. Otsuka, T. Kudo : Hot Corrosion of Commercial Tube Steel Materials in a Japenese Waste Incinerator Environment, High Temperature Corrosion of Advanced Materials and Protective Coatings, Amsterdam, The Netherlands, Elsevier Science Publishers, 1992.205.

58. Dongbai XIE, Fuhui Wang. J. Mater. Sci. Technol., 2003.19.

59. Pilling NB, Bedworth RE. J. Inst. Met, 1923.29: P. 529.

60. ASM Handbook Vol.13 Corrosion, ASM International, 1987.

VITAE

Name Adeel Khalid

Date of Birth 7th October 1986

Nationality Pakistani

Religion Islam

Educational Qualifications

i) B.S. Metallurgical and Materials Engineering from Ghulam Ishaq Khan Institute of Engineering Sciences and Technology, Pakistan, 2008.

ii) M.S. in Mechanical Engineering, KFUPM, June 2011.

Present and Permanent Address

41-A Judicial Employees Colony, Phase 1, Lahore, Pakistan.

Mobile Numbers +966568833725

+923214045089

Email address Khalid.adeeL7@gmail.com